SF 298 MASTER COPY KEEP THIS COPY FOR REPRODUCTION PURPOSES

REPORT DOCUMENTATION PAGE

Form Approved OMB NO. 0704-0188

1. AGENCY USE ONLY *(Leave blank)*	2. REPORT DATE	3. REPORT TYPE AND DATES COVERED
	10/96	Technical Report 4/96-10/96

4. TITLE AND SUBTITLE

InAsSb(P)-InAsSb-InAs Long Wavelength Lasers

5. FUNDING NUMBERS

DAAH04-95-1-0343

6. AUTHOR(S)

M. Razeghi, J. Xu, S. Kim, D. Wu, M. Erdtmann, J. Kim, E. Michel, B. Lane, A. Rybaltowski, J. Diaz, Y. Xiao, V. Litvinov, H-J Yi

7. PERFORMING ORGANIZATION NAMES(S) AND ADDRESS(ES)

Northwestern University
Center for Quantum Devices
2225 N. Campus Drive, Room 4051
Evanston, IL 60208-3118

8. PERFORMING ORGANIZATION REPORT NUMBER

9. SPONSORING / MONITORING AGENCY NAME(S) AND ADDRESS(ES)

U.S. Army Research Office
P.O. Box 12211
Research Triangle Park, NC 27709-2211

10. SPONSORING / MONITORING AGENCY REPORT NUMBER

ARO 34373.3-PH

11. SUPPLEMENTARY NOTES

The views, opinions and/or findings contained in this report are those of the author(s) and should not be construed as an official Department of the Army position, policy or decision, unless so designated by other documentation.

12a. DISTRIBUTION / AVAILABILITY STATEMENT

Approved for public release; distribution unlimited.

12 b. DISTRIBUTION CODE

13. ABSTRACT *(Maximum 200 words)*

We have grown InAsSb/InAsSbP DH laser structures and InAsSb/GaSb superlattices on InAS substrates. Our V/III ratio is between 40-100 for both the active and cladding layers, and the growth rate is 1.0 um/hr, which resulted in a mirror-like surface morphology. The x-ray FWHM is 46 arc s. for the InAsb layer and 79 arc s. for the InAsSbP layer. PL intensity is unchanging up to 200 K and remains strong up to room temperature. We have investigated the influences of growth conditions on the material parameters as well as examined the causes for non-radiative recombination, and have deduced that it mainly originates from the InAsSb/InAsSbP heterointerfaces, though our material has demonstrated increased radiative efficiency at tempratures up to 200 K.

14. SUBJECT TERMS

15. NUMBER IF PAGES

16. PRICE CODE

17. SECURITY CLASSIFICATION OR REPORT	18. SECURITY CLASSIFICATION OF THIS PAGE	19. SECURITY CLASSIFICATION OF ABSTRACT	20. LIMITATION OF ABSTRACT
UNCLASSIFIED	UNCLASSIFIED	UNCLASSIFIED	UL

InAsSb(P)-InAsSb-InAs Longwavelength Lasers

ARPA/US Army Project # DAAH04-95-1-0343

Principal Investigator: Manijeh Razeghi

Center for Quantum Devices
Northwestern University, Evanston, IL 60208

Period covered by report: April 1996 - October 1996

Scientific Personal:

MOCVD and MBE growth:

Staff: Dr. J. Xu
Students: S. Kim, Di Wu, M. Erdtmann, J. Kim
E. Michel, B. Lane

Laser Processing and Measurements:

Staff: Dr. J. Xu
Students: A. Rybaltowski, J. Diaz, Y. Xiao

Theorectical Calculations: Staff: Dr. V. Litvinov Student: H.-J. Yi

DISCLAIMER NOTICE

THIS DOCUMENT IS BEST QUALITY AVAILABLE. THE COPY FURNISHED TO DTIC CONTAINED A SIGNIFICANT NUMBER OF PAGES WHICH DO NOT REPRODUCE LEGIBLY.

Chapter 1. The growth and characterization of InAsSb / InAsSbP by LP-MOCVD.

Outline

Summary

I. Introduction

II. InAsSb/ InAsSbP double heterostructure grown on (100) InAs.

2.1 Growth Condition

2.2 Results

2.3 N- and P-doping for InAsSbP.

III. The study of the Heterointerface characteristics of Sb based materials.

3.1 The characteristics of InAsSb/InAsSbP heterointerfaces.

3.2 GaSb/InAsSb superlattice.

Summary

We have grown InAsSb/InAsSbP DH laser structures and InAsSb/GaSb superlattices on InAs substrates. Our V/III ratio is between 40-100 for both the active and cladding layers, and the growth rate is 1.0 μm/hr, which resulted in a mirror-like surface morphology. The x-ray FWHM is 46 arc s. for the InAsSb layer and 79 arc s. for the InAsSbP layer. PL intensity is unchanging up to 200 K and remains strong up to room temperature. We have investigated the influences of growth conditions on the material parameters as well as examined the causes for non-radiative recombination, and have deduced that it mainly originates from the InAsSb/InAsSbP heterointerfaces, though our material has demonstrated increased radiative efficiency at temperatures up to 200 K.

I. Introduction

It is well known that the mid-infrared wavelength range from 3-5 μm is very attractive for several spectroscopic applications including atmospheric trace gas analysis and medical diagnostics, because in this spectral region many atmospheric species have strong rotational, vibrational, and overtone absorption bands. Unfortunately, the performance of narrow band-gap semiconductor lasers is strongly influenced by Auger processes and carrier leakage effects.

We reported the high quality of double heterostructure laser diodes based on the $InAs_{0.95}Sb_{0.05}/InAs_{0.40}Sb_{0.22}P_{0.38}$ alloy on InAs substrate (100) grown by MOCVD which shows the lowest threshold current density and highest output power ever reported. However the dominant nonradiative recombination with higher temperatures limits the operating temperature of the laser diodes. Our work has been to concentrate on optimizing the growth conditions and investigating the fundamental mechanisms of suppressed radiative recombination at high temperatures to obtain high quality material to overcome these problems and also to develop the proper structure for better carrier confinement. We showed already the radiative transitions are the dominant mechanism up to 200K, depending on the material quality, at high output power, which is also important to obtain low detection limits and high time resolution.

We developed the quaternary material based on phosphorous, i.e. $InAs_yP_xSb_{1-x-y}$ lattice matched to $InAs_{1-x}Sb_x$ on (100) InAs substrate grown by low pressure MOCVD as reported in previous works. The benefit of this material system is that the composition x of $InAs_{1-x}Sb_x$ can be easily varied, which means we have a variable emitting wavelength for a broad range above 3 μm, depending on x.

II. InAsSb/InAsSbP Double Heterostructure grown on (100) InAs.

2.1 Growth condition.

Samples were grown in a horizontal, cold-wall, quartz tube low pressure metalorganic chemical vapor deposition (LP-MOCVD) reactor at a pressure of 78 torr. The precursor sources are trimethylindium (TMIn), trimethylantimony (TMSb), and both pure and diluted arsine (AsH_3) and phosphine (PH_3). Diethylzinc (DEZn) and Tetraethyltin (TESn) are used for p-type and n-type doping, respectively. The growth temperature was varied from 460°C to 510°C in order to obtain a high-quality InAsSb active layer. The growth rate has approximately a linear relationship with the mass flow of TMIn, which indicates a diffusion-limited process in this temperature range.

The V/III ratio is also very critical in growing InAsSb(P) alloys. For the active layer, the V/III molar gas flow ratio is varied between 40 to 100, keeping the same composition x of $InAs_xSb_{1-x}$ and $V_{AsH3}:V_{TMSb} \approx 2.8:1$ for a Sb composition of 5 ~ 6 %. For the upper and lower cladding layers, the V/III molar gas flow ratio is also about 70 and the growth condition was varied with the ratio of flow rate of As/Sb, As/P, and Sb/P. The growth condition was optimized to improve the crystalline quality, increase the energy gap, and to make sharp interfaces between InAsSb/InAsSbP. Due to the different thermal stabilities for precursors PH_3 and TMSb and different sticking coefficients of elemental phosphorous and antimony on the semiconductor surface, it is critically important to find the proper flow rate and the growth temperature. The stable hydride PH_3 requires a much larger residence time for efficient cracking in the hot zone above the susceptor than the less stable TMSb. It causes difficulties in controlling the relative rates of incorporation of P and Sb into the solid. And it is well known that when during the growth of Sb-containing materials, the excess of Sb will generate droplets on the sample surface and give a very

rough surface morphology. In our growth of InAsSb and InAsSbP, the group V composition is dominated by As and P. The much stronger As and P driving force for incorporation prevents the excess Sb from bonding with the sample surface, thus no Sb droplets are generated. A high flow rate of TMSb is helpful to obtain a smooth surface and high crystal quality. The growth rate, another important parameter, was varied between 0.8 μm/hr and 1.5 μm/hr. The lowering of the growth rate will improve the crystal quality; we employ a growth rate around 1 μm/hr to compromise both the total growth time for the relatively thick layers and the crystalline quality.

2.2 Results

Prior to loading into the reactor chamber, the n-type (100) InAs substrates were degreased with organic solvents and etched with a H_2SO_4:H_2O_2:H_2O solution. The laser structure is composed of an $InAs_{0.95}Sb_{0.05}$ buffer layer and an $InAs_{0.95}Sb_{0.05}$ active layer. The active layer is sandwiched between $InAs_{0.40}Sb_{0.22}P_{0.38}$ upper and lower cladding layers. All the epitaxial layers have a 0.35% lattice mismatch with the InAs substrate but are lattice matched to each other. The composition of each layer is determined from x-ray diffraction and PL spectra. Fig. 1 schematically shows the structure of the DH sample. The upper and lower cladding layer thicknesses are each about 1.4 μm and the active layer thickness is about 1.2 μm, measured by both ball polishing and scanning electron microscopy (SEM).

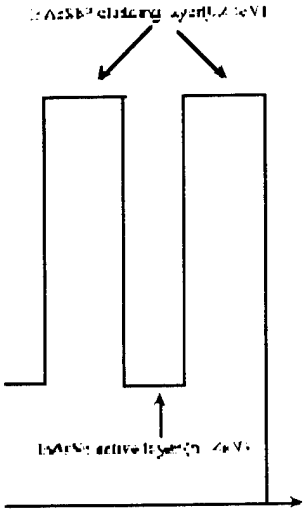

Figure 1. The schematic structure and energy gap of a DH laser structure

With the proper growth conditions, the x-ray diffraction spectrum of the InAsSb and InAsSbP epilayers in Figure 2 shows very sharp peaks from each layer such as 46 arcsec of InAsSb and 78 arcsec of InAsSbP. It indicates the improvement of the material quality compared to the previous work by changing the growth parameters to figure out the proper Sb incorporation.

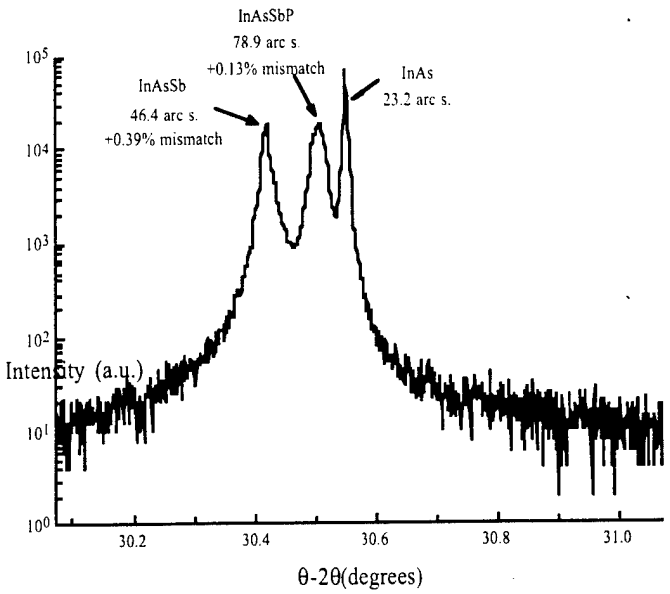

Figure 2. Typical X-ray diffraction spectrum of a double heterostructure.

It is not clearly explained yet the reason of the dropping of the photoluminescence intensity of the epilayer which is expected depending on the material quality. To investigate the dominant mechanism of suppressed radiative recombination causing the rapid dropping of the intensity with increasing temperature, several structures were grown and measured. The reason can be expected as trapping at impurities, localization at heterointerfaces and the different mechanisms of scattering. The typical photoluminescence spectrums of the double heterostructure are given in figure 3.

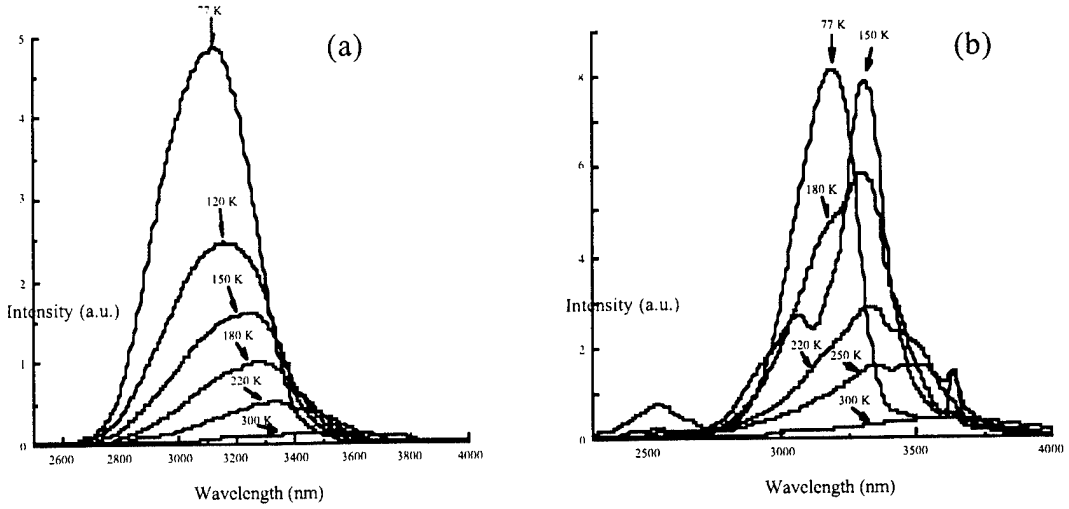

Figure 3. The typical photoluminescence spectrum of laser (a) and DH structure (b).

The luminescence intensity does not drop up to 200K which means that the high quality material reduces the nonradiative recombination center and accordingly the efficiency of the radiative recombination is increased up to this temperature. We expect that the thermally ionized impurities and dominant carrier leakage cause the broadening of the PL spectrum line and it can be one of the main reasons for the relatively rapid dropping of the intensity at high temperature. From these results, we expect the better heterointerface between InAsSb and InAsSbP, which can be the critical center for the nonradiative recombination such as band-to-trap recombination.

2.3 N- and P- doping for InAsSbP

For narrow-gap semiconductors it is well known that they are unintentionally doped n-type with carrier concentration around ~10^{16}. It shows the difficulty to control the doping concentration because it depends on many factors such as the flow rate, V/III ratio,

and temperature. Relatively lower growth temperature required for InAsSbP or InAsSb causes the higher ratio of the incorporation of Zn for P-type doping compared to Sn for N-type doping, which is more stable with temperature. The control of the carrier concentration is more important for narrow gap semiconductors because the Auger lifetime can be comparably decreased with higher carrier concentration as already calculated. It shows that the Auger coefficient could be increased by a factor of 100 by increasing the carrier concentration from 10^{17} to 10^{18}. Our experiments show the similar results of decreasing of the efficiency of the radiative recombination with relatively higher p-doping concentration. In Figure 4, we show the doping effect of this structure which examines the possibility of the dominant Auger recombination with the effectively higher carrier concentration. The photoluminescence intensities were measured with varying temperature. The temperature dependence of the integrated peak intensity was plotted for three different doping characteristics and the data was fit to the function.

$$I(T) = \frac{I(0)}{1 + C\exp(-E_a / kT)}$$

where C is a constant, and $E_a \approx (m_e/2m_{hh})Eg$ is the thermal activation energy which is related to the Auger threshold energy. The fitted value of E_a for the undoped and n-doped material (E_a=40 meV) is relatively lower than that of the p-doped material (E_a=60 meV) from which we can estimate relatively higher carrier concentrations cause the lower intensity with increasing temperature due to the dominant nonradiative recombination specified as the Auger effect because we can expect the same condition for the interface between InAsSb and InAsSbP, and eliminate the effect of the heterointerface such as the trap or localization from interfacial defects.

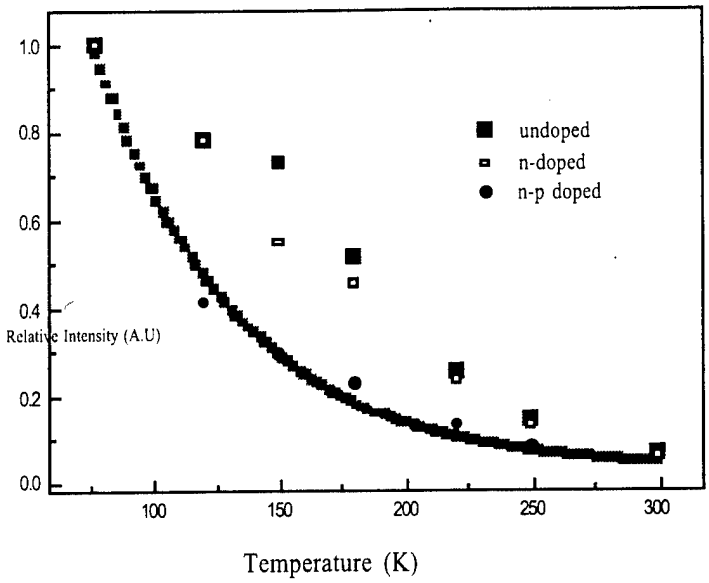

Figure 4. Temperature dependent luminescence intensity with different doping profile.

However, it is interesting that above the critical temperature (around 220K), we cannot find any difference among all three of the structures. It can be evidence of the carrier leakage due to the relatively lower energy gap of the confinement layer InAsSbP which has a saturated energy gap range in our growth system. And it shows that the carrier confinement becomes more important as increasing temperature due to the thermalized effect of the carriers.

III. The study of the Heterointerface characteristics of Sb based materials.

3.1. The characteristics of InAsSb/InAsSbP Heterointerfaces.

One of the indicating problems of InAsSb and InAsSbP double heterostructure is the interface between these two layers. For laser structures, we need to grow relatively thick active layers to avoid the diffusion of the defects through the interface. Even though there are difficulties to control the interface due to the limitation of the reactor, we set the growth conditions as keeping the TMIn and TMSb flow rates as constant as we can. Actually the switching sequence and the time delay are important factors to control the composition due to the comparably different Sb and P incorporation ratios and the sticking coefficient causing more difficulties for growing InAsSbP. Our first work is to examine the effect of the total hydrogen flow rate on the growth condition and to compare the difference using photoluminescence. The different intensities and spectra were given in figure 5 with four samples grown with different total flow rates. The samples were measured at the same time with the same excitation power to compare their differences more precisely. The luminescence intensity is relatively strong and the FWHM of the spectrum is narrower with lower flow rate, which is more apparent at lower temperatures. We observe the separate peak comes apart from the main peak, which can be interpreted several ways, but it seems to be more related to the interface between the active layer and quaternary cladding layer.

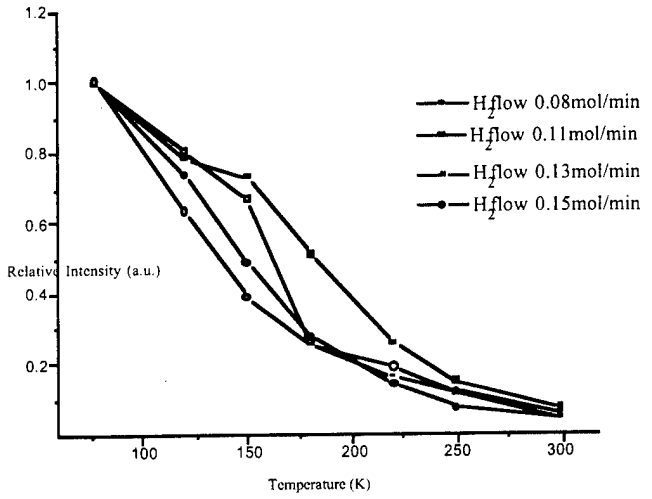

Figure 5. Photoluminescence measurement depending on the total H_2 flow rate

As seen from the figure, the separation of the peak appears more dominantly with increasing total flow rate. The peaks are regularly separated as nearly $\Delta E \approx 2kT$ from the main luminescence peak. The area nonuniformity and the compositional inhomogeneities are the other main characteristics of the InAsSb epilayer which may not provide sufficient gain to produce lasing as well as account for the variation of the emitting wavelength. The flow rate and the growth temperature can significantly affect these characteristics which is related to the ordering of the Sb-based materials and determine the device performance properties.

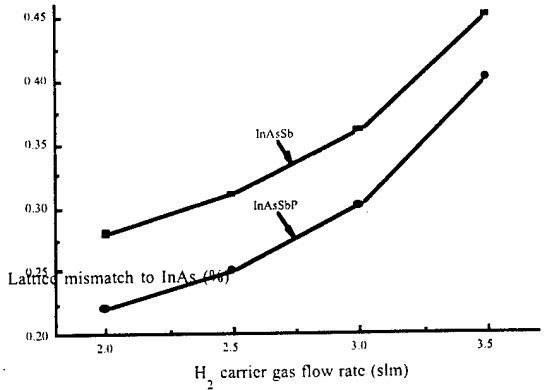

Figure 6. Lattice mismatch of InAsSb and InAsSbP compared to InAs as a function of carrier gas flow rate.

Fig. 6 shows the mismatch of both the InAsSb and InAsSbP layers to the InAs substrate as a function of carrier gas flow rate. The graph reveals a superlinear dependence of the mismatch on the flow rate for both InAsSb and InAsSbP. Since the lattice constant of these materials is dependent solely on the group V composition ratios, because there is no group III intermixing, then the ratios of group V incorporation will be the only factor affecting the epilayer mismatch. Due to the same mismatch dependence on the carrier gas flow rate, then the presence or absence of PH_3 has no bearing on this result, therefore the P incorporation is practically independent of carrier gas flow rate.

For the remaining two species, Sb and As, we notice that the mismatch increases with increasing flow rate. This means either the Sb becomes more incorporated or the As becomes less incorporated into the material, because InSb has a larger lattice constant than either this ternary or quaternary while InAs has a smaller lattice constant than either. Since the higher carrier gas flow rate decreases the residence time of a species over the substrate, thus lowering the incorporation of that species, then the dependency of the mismatch on the carrier gas flow rate is a result of decreased As incorporation.

3.2 GaSb/InAsSb superlattice.

There is increasing interest in type II superlattices for potential LWIR detectors and light emitting diodes due to the flexibility of the effective energy gap and refractive indices, and the specific band alignment which causes the hole and electron localization. We grew the GaSb/InAsSb superlattice to examine how Sb works as a group V element and how we can control the interface with Sb-based materials because superlattices have a large number of heteroepitaxial interfaces which are easily analyzed using the interference from x-ray diffraction. Compared to GaAs and InGaP, which shows the possibility of the large degree of crystalline perfection due to the progress in epitaxial growth techniques, the characterization and simulation of these Sb-based superlattices, which are usually aligned as type II, have not been widely reported. The 20 period GaSb/InAsSb superlattice was grown by LP-MOCVD and measured with high resolution x-ray diffraction, and at the same time the dynamic simulation of this materials was studied. Both (004) and (335) diffractions are measured to study the structural parameters of the samples. GaSb and InAsSb have around a 0.3% lattice mismatch with each other that causes the asymmetric fringes of the diffraction pattern, which is more obvious in the (335) geometry. The control of the switching time between Sb and As of the InAsSb epilayers has an effect on the number of fringes and the degree of sharpness of the diffraction pattern. Sb is relatively heavy compared to the other group V precursors, and its incorporation is dependent on the vapor velocity of the flow rate which forms the interface between InAsSb and GaSb. From switching GaSb to InAsSb, the excess of Sb still remained with the desorbed Sb, which has a higher desorption ratio, thus it needs the proper time of the access of As. The simulation of InAsSb/GaSb superlattices and the x-ray diffraction spectrum are given in

Figure 7. In Figure 8, the scanning electron microscope image of the cross section of these layers are shown.

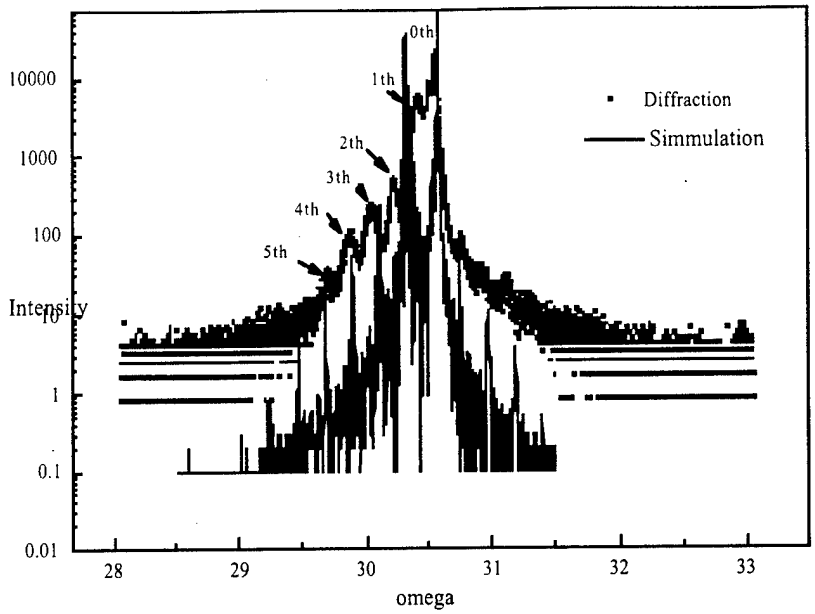

Figure 7. X-ray diffraction and simulation of InAsSb/GaSb superlattice.

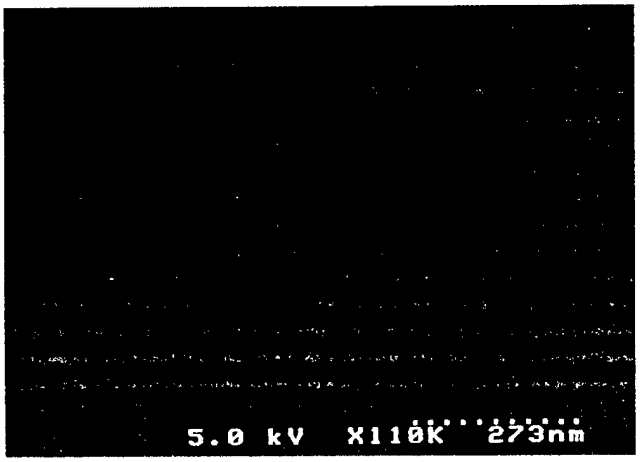

Figure 8. SEM image of a cross section of a InAsSb/ GaSb superlattice

Chapter 2 MOCVD growth and characterization of mid-infrared laser structur
From Di Wu & Brett Lane
EMCORE

2.1 optimization of reactor carrier gas flow rate and rotation rate of sample holder

GaInP /GaAs are grown as calibration samples.

For each growth, sample "A" is at the center of the sample holder and sample "B" is in the "square" at the edge of the sample holder.

a) Total flow rate of gas to the growth chamber is 27 l/min.

Rotation of sample holder is 1000 rpm.

Sample #	X-ray FWHM GaAs (sec)	GaInP	GaInP/GaAs mismatch difference between two points 1cm apart	Mismatch difference between sample A and B	Growth rate of GaInP (A/min)	Morph ology
A	22	47	0.024%	--------	108	ok
B	27	49	0.019%	0.017%	113	ok

Note: Growth rate is low and the uniformity is ok across the samples and from sample to sample.

b) Total flow rate of gas to the growth chamber is 14 l/min

Rotation of the sample holder is 1000 rpm

Sample #	X-ray FWHM GaAs (sec)	GaInP	GaInP/GaAs mismatch difference between two points 1cm apart	Mismatch difference between sample A and B	Growth rate of GaInP (A/min)	Morph ology
A	21	42	0.029%	--------	163	ok
B	24	40	0.045%	0.015%	175	ok

Note: Growth rate increased due to the decrease of total carrier gas flow rate which causes the sources to be less dilute in the growth chamber. The uniformity is ok.

c) Total flow rate of gas to the growth chamber is 14 l/min

Rotation of the sample holder is 500 rpm

Sample #	X-ray FWHM GaAs (sec)	GaInP	GaInP/GaAs mismatch difference between two points 1cm apart	Mismatch difference between sample A and B	Growth rate of GaInP (A/min)	Morph ology
A	23	61	0.05%	---------	110	a few defects
B	19	58	0.06%	~0.2%	98	a few defects

Note: The growth rate decreased due to the decrease in the rotation rate of sample holder. The uniformity is not good and there is a big composition difference between different samples that had been grown at different positions on the sample holder.

d) Conclusion

When total flow rate of the carrier gas to the growth chamber is 14 l/min. and rotation rate of sample holder is 1000 rpm , good sample quality with a fair growth rate can be achieved.

2.2 Doping

Control of the doping level for the laser structure is critical for laser operation. Since there is not a more reliable way to measure the carrier concentration in InAsSb or InAsSbP narrow bandgap material grown on n^+ -InAs substrate, we did the doping calibration on GaAs samples with an etching profiler which not only gives the doping level but also the doping profiles through all the epi-layers so as to tell the uniformity of doping.

With the EMCORE reactor, we can easily dope GaAs up to 10^{20} cm^{-3} with DeZn and up to $-5*10^{19}$ cm^{-3} with TESn.

Because doping level is very sensitive to growth temperature , all the GaAs samples are doped at 580°C (as measured by the thermocouple, the real temperature is about 520°C as measured by the calibrated pyrometer). This is close to the growth temperature of InAsSb/InAsSbP laser structures, which makes the calibration more reliable.

a) p-type

DeZn is used as the source for p-type doping. The pressure inside the DeZn bubbler is chosen to be 700 torr and the bubbler's temperature is -14°C .

Since the vapor pressure of Zn is high, most of the Zn reaching the sample surface will be reevaporated, instead of being incorporated into the epi-layers. Therefore the carrier concentration is proportional to the DeZn flow rate but exponentially decreases with temperature as shown in the following figures.

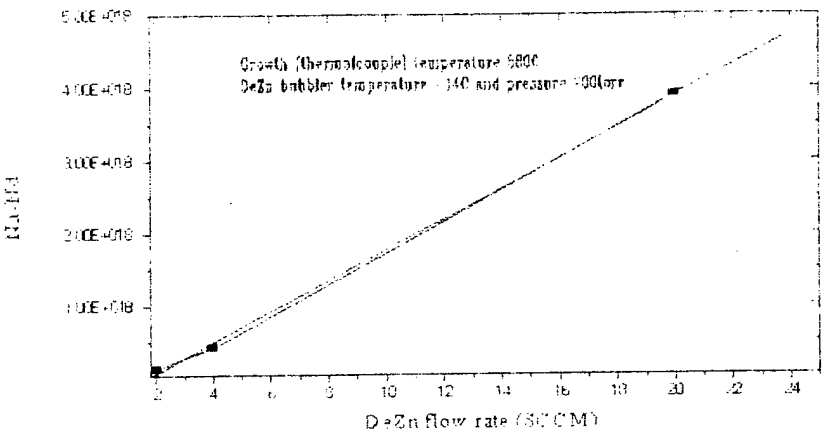

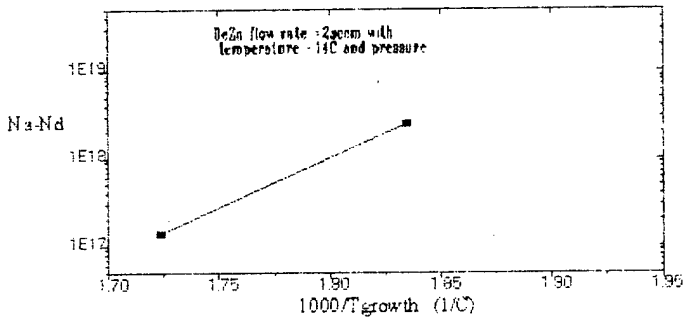

b) n-type

TESn is used as the source for n-type doping sources. The pressure of the TESn bubbler is 700 torr and the bubbler's temperature is -5°C. Doping is achieved when Sn replaces the group III element position . Basically, the doping level is proportional to the P(TESn)/P(III), where P(TESn) and P(III) are the partial pressures of TESn and the group III OM sources at the sample surface respectively. During the whole growth the group III OM flow rate is kept constant, thus the doping level is directly proportional to the TESn flow rate. The effect of temperature on doping is through cracking TESn, so that the higher the temperature, the more TESn cracked and the higher the doping level. The following figures show the carrier concentration as a function of TESn flow rate and of temperature.

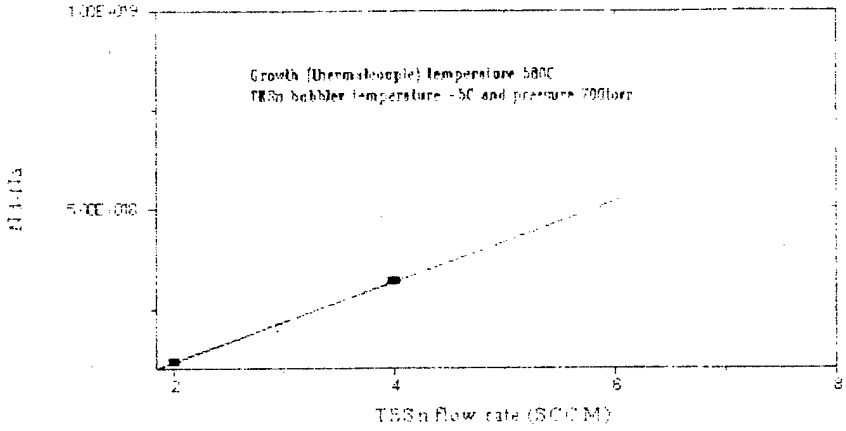

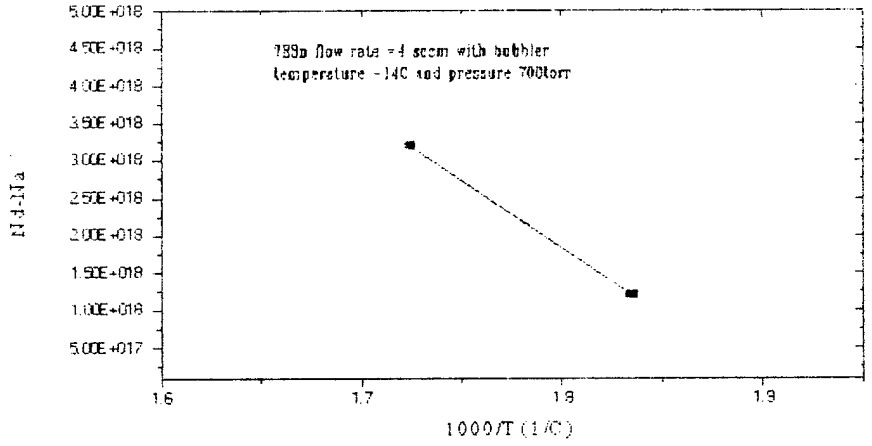

2.3 Optimization of InAsSb layer

In the laser structure, the InAsSb layer is the active layer. Its crystal and optical quality is extremely important for the performance of laser diodes. Growth conditions are optimized in order to get a high quality InAsSb layer.

a) Growth temperature.

Growth temperature has been varied from 450°C to 530°C. The FWHM of the x-ray and PL peaks from the InAsSb epitaxial layers as a function of growth temperature are shown in the following:

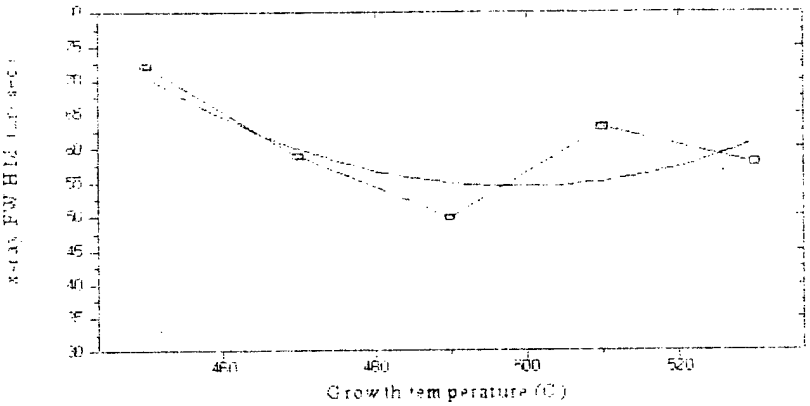

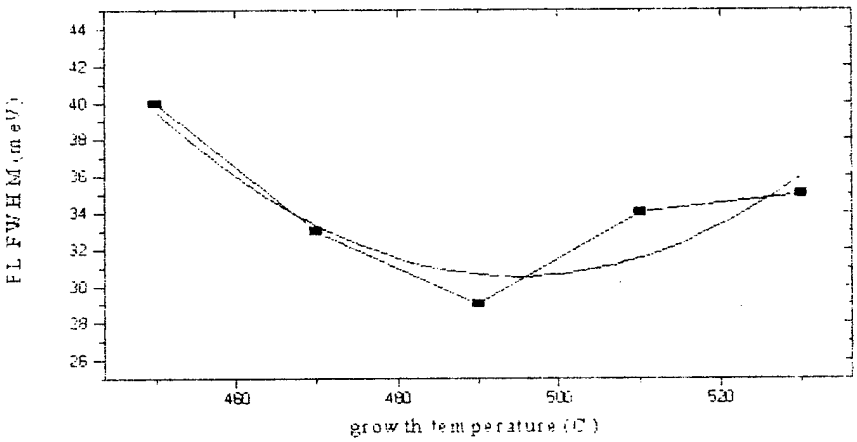

We can see from the figures that the crystal quality and the optical quality are closely related. At about 490°C the InAsSb has the best crystal and optical quality. At this temperature the morphology of this sample is mirror like.

b) Growth rate

The growth rate as a function of temperature is shown below:

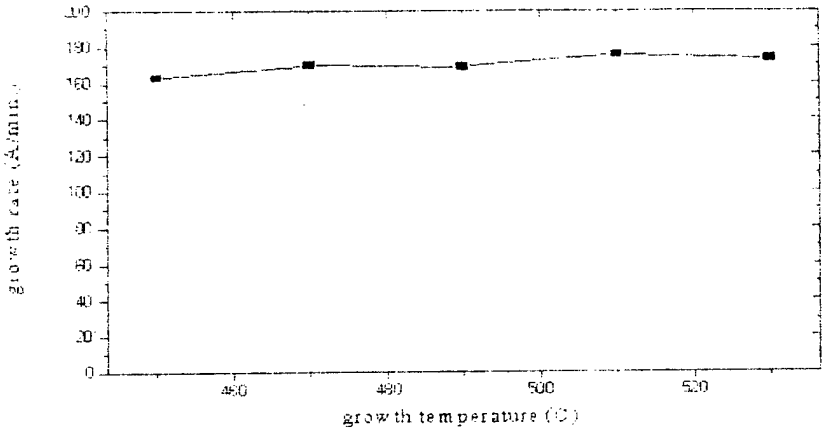

In the temperature range from 450 to 530°C, the growth rate is roughly independent of temperature, indicating that the growth is diffusion limited and good for uniform growth. In other words, the layers will grow at a uniform rate even when there is a temperature gradient around the surface of the sample.

c) V/III ratio

The V/III ratio is another critical parameter for growth, especially for antimony based growth.

Too high a V/III ratio will cause an excess of antimony on the sample surface and drops of antimony may be generated thus causing a rough surface. The antimony problem is not so serious for our growth, because the group V composition of our InAsSb layers is only 5% antimony. In addition, it seems that a high flow rate of AsH_3 during growth prevents the generation of Sb drops on the sample surface even when we flow much higher amounts of Sb than required.

On the other hand, too low a V/III ratio will lead to unstable growth and will give bad crystal quality. Therefore, a certain amount of AsH_3 is required in order to get a V/III ratio which is high enough to avoid this problem.

The following is the x-ray FWHM as a function of the V/III ratio.

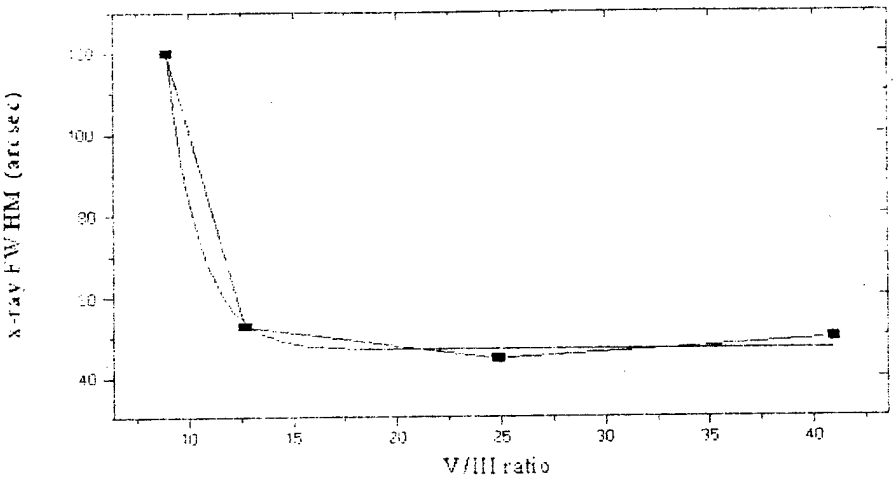

On the high V/III ratio side, the x-ray FWHM is almost constant. But on the low V/III ratio side, the crystal quality decreases rapidly. This result suggests that the V/III ratio should be no lower than 15.

d) The growth rate and stabilization of the growth.

The growth rate should be properly chosen in order to have the overall best quality of the InAsSb epi-layers.

The x-ray FWHM as a function of growth rate is shown below:

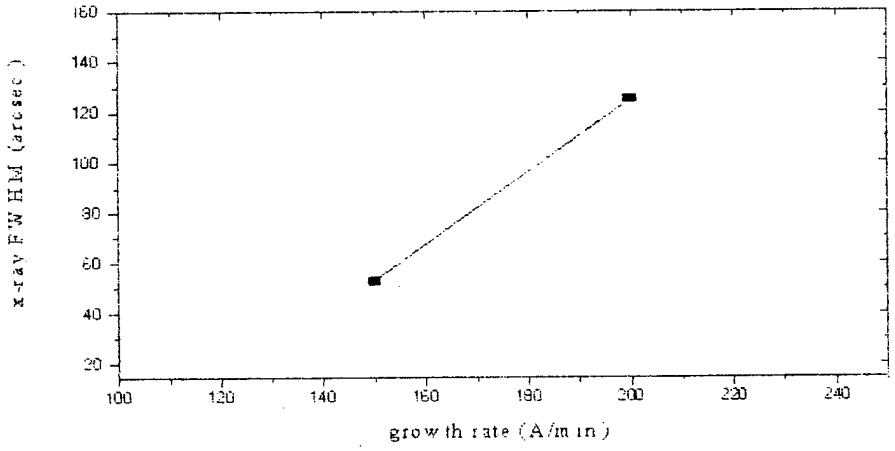

This means that better crystal quality is obtained with a low growth rate. However, a long growth time is required for a very low growth rate, which is not good because the x-ray FWHM becomes larger as the growth time becomes longer as shown below. This indicates an unstable growth if the growth time is too long.

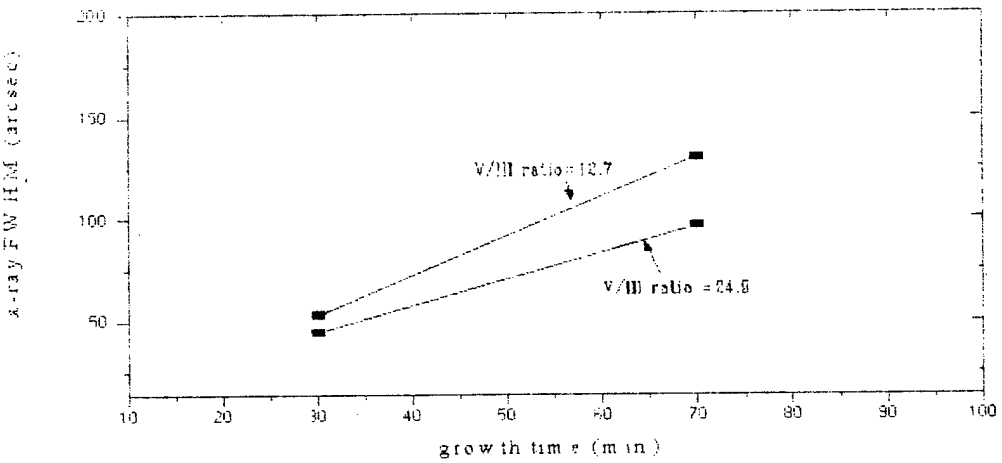

The reason is two fold: firstly, the fluctuation and slow drift of the V/III ratio for a long growth time causes the InAsSb composition to change. This effect is not avoidable. Secondly, during growth the growth temperature slowly changes due to deposition on the sample holder which changes the thermal equilibrium pattern and radiation on its surface. Since deposition on the sample holder is unavoidable, this effect also is unavoidable.

As a compromise to the above two considerations, the growth rate of the InAsSb layer is chosen to be about 150A/min. After properly adjusting the growth condition, we get pretty good x-ray for a 70 minute long growth.

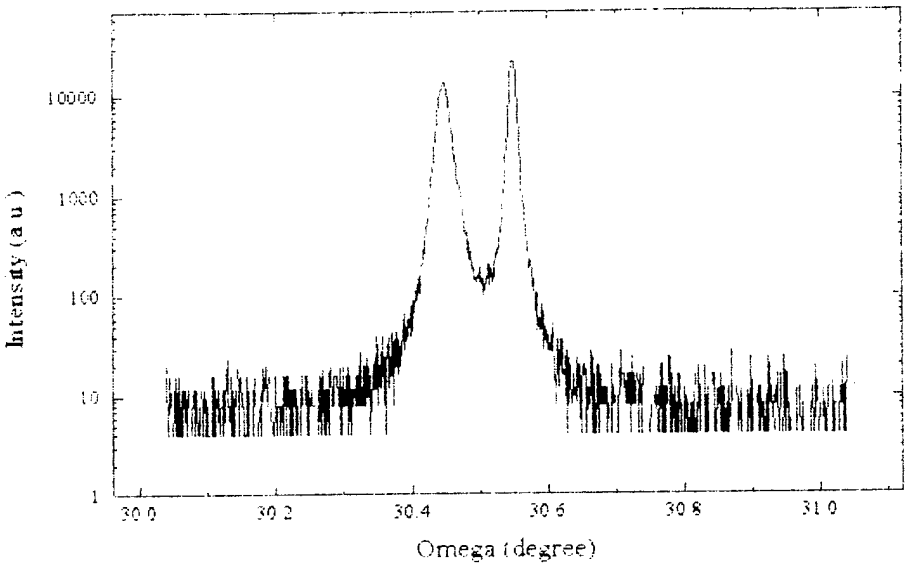

2.4 PL investigation of the DH Laser structures

The typical DH structure we grew for mid-infrared laser is the following:

p-type InAsSbP upper cladding layer
InAsSb or InAs active layer
n-type InAsSbP lower cladding layer
n-type buffer layer
n^+ InAs Substrate

Our PL results are from the following laser samples grown on the EMCORE reactor: sample #40, #92, #99 and #94. Samples #40, #92 and #99 are InAsSbP/InAsSb/InAsSbP DH structure grown on InAs (100) substrates and sample #94 is InAsSbP/InAs /InAsSbP DH on InAs(100) substrates. The main parameters of these sample are shown in table 1.

Table 1 The main parameters of the samples:

Sample #	Lower cladding layer thickness (μm)	Active layer thickness (μm)	Upper cladding layer thickness (μm)	Mismatch between DH structure and InAs substrate	Growth temperature (°C)	Cladding layer barrier height, ΔE_v at 80K (meV)
40	1.21	0.91	1.20	0.35%	465	96.6
92	1.29	1.09	1.389	0.371%	520	98.6
94	1.15	0.95	1.211	0.046%	520	98.7
99	1.2	1.13	1.354	0.34%	520	125.2

In order to make a mid-infrared laser operate at room temperature, it is very important to understand its PL performance as a function of temperature and to find the major factors that limit the maximum operating temperature.

The following two figures show the PL intensity of sample #99 at different temperatures and the normalized PL intensity as a function of temperature for all the samples.

First of all, we can see the PL intensity of sample#99 is strong up to room temperature and the room temperature PL intensity is only 8 times lower than that at 80K. It is much better than the typical results from InAsSb/InAsSbP DH samples.

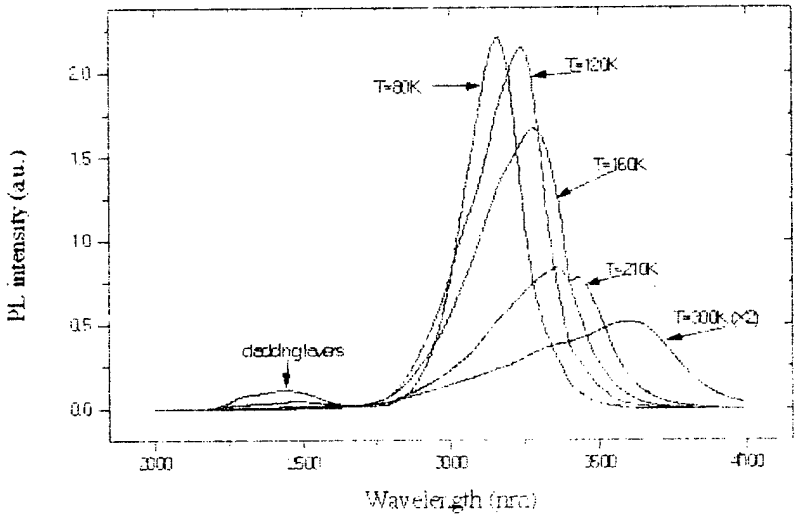

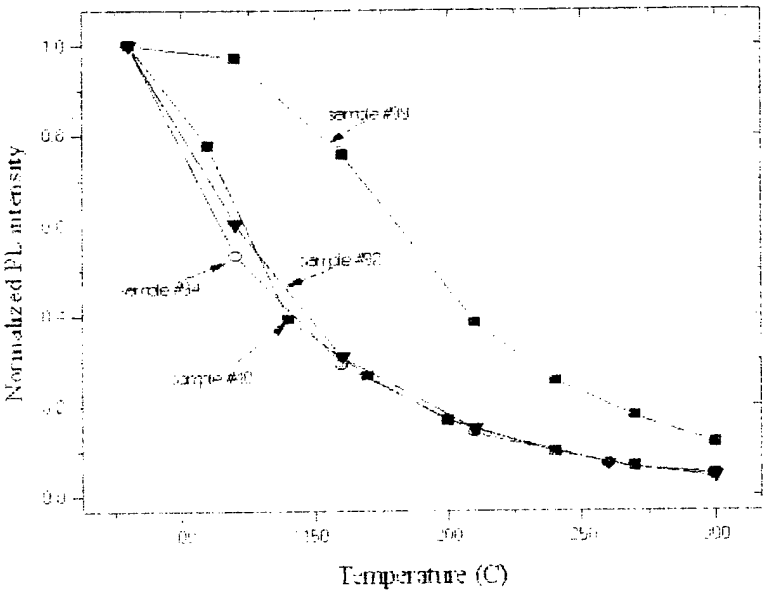

Now let us focus on the second figure. First, take a look at the intensity -temperature curves (or more simply the I-T curves) corresponding to sample #40 and sample #94, which have almost the same parameters but different growth temperatures of 465°C and 520°C respectively. Their identical PL intensities as a function of temperature suggest that at least in the range from 465°C to 520°C, the growth temperature has no obvious effect on I-T performance.

Comparing the I-T curves of sample #92 and sample #94, we find out that they are also very close, which indicates two things. Firstly, the mismatch dislocation is not the main factor to determine how PL intensity decreases with increasing temperature because in sample #94 the cladding layers and active layer are almost lattice matched with the InAs substrate and in sample #92 the eptiaxial layers have 0.371% mismatch with InAs substrate. If mismatch dislocation were a major factor, sample #92 should have a much worse temperature dependence of PL intensity. Secondly, we can rule out the possibility that phase separation and nonuniform growth of the InAsSb active layer in sample #92 is the key factor to determining the temperature dependence of PL intensity because the active layer of sample #94 is InAs which does not have the problem of phase separation and nonuniform growth, yet has the same I-T performance as sample #92.

Auger recombination is an important factor for long wavelength lasers. It is believed that it is the dominate factor that limits the maximum operating temperature for mid-infrared lasers. However our PL data suggest that there is another factor as important as Auger recombination which determines the sample's temperature dependence at this stage.

However our PL data suggest that there is another factor as important as Auger recombination which determines the sample's temperature dependence at this stage.

In our PL data, we find that the I-T curve is very different between sample #99 and samples #40, #92 and #94, and this same kind of difference is also found in our other samples. Because Auger recombination is an intrinsic process, its effects should be about the same for sample with identical active layers. However, this is not the case in our data. Therefore there must be another parameter that is responsible for the difference in PL data between sample #99 and samples #40, #92 and #94..

The other data also supporting the above argument are shown in the following figures.

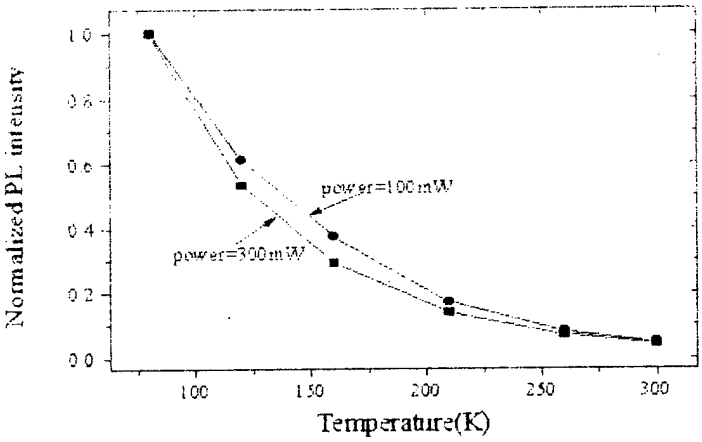

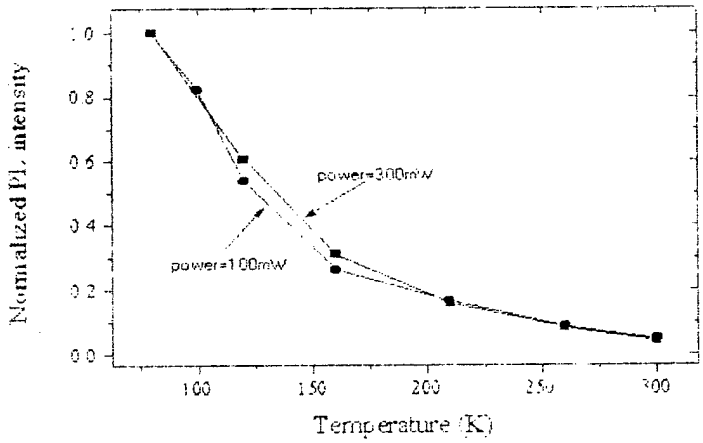

recombination $\propto n^2$ and Auger recombination $\propto n^3$ where n is the carrier concentration. Different laser excitation powers will give different n. If the radactive and Auger recombination are the only two dominant factors to determine PL intensity, then the I-T performance of the samples will be much different at different laser excitation powers. However, from the figures above we can see that the temperature dependence of PL intensity is identical at different laser excitation powers for both InAs and InAsSb active layers.

The parameter whose change causes obvious I-T change is the cladding layer barrier height. This indicates that the spilling of carriers out of the active layer is one of the major factors to determine the I-T curves for the InAsSb/InAsSbP material system.

As far as we know for the InAsSb/InAsSbP material system, the highest barrier height (ΔE_g) with decent InAsSbP epi-layer quality is less than 150meV. Effort has been put on the growth of InAsSbP with even higher bandgap . Other materials, such as InAlAsSb, with high bandgap have also been tried.

2.5 The other suggested structures to approching longer wavelength and higher laser operational temperature

a) GaInSb/InAsSb/GaInSb DH growth on GaSb substrate which gives 4.6μm PL peak at 80K

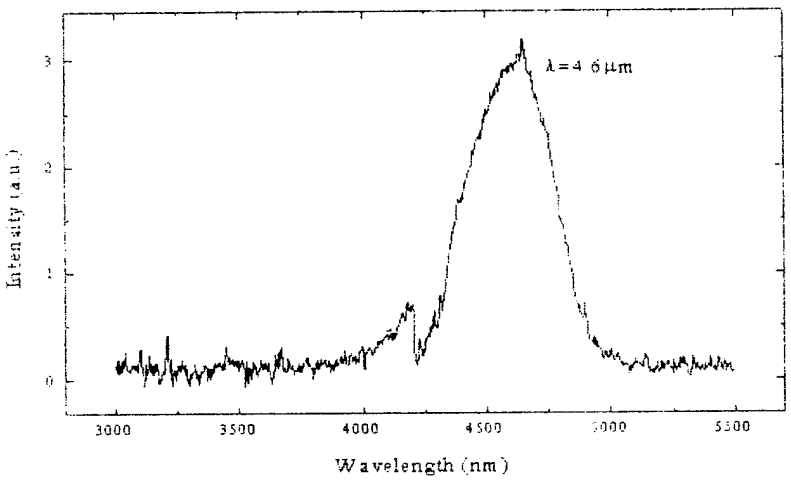

b) PL from InAsSbP/grading InAsSb /InAsSbP for the wavelength more than 4μm.

The composition of InAsSb active layer can be tuned to get longer emission wavelength than 4μm. However it has large lattice mismatched with the InAs substrate. To avoid dislocation defects generated from the interface between epi-layers and InAs substrate, grading InAsSb active has been grown. The structure and PL result are shown followings:

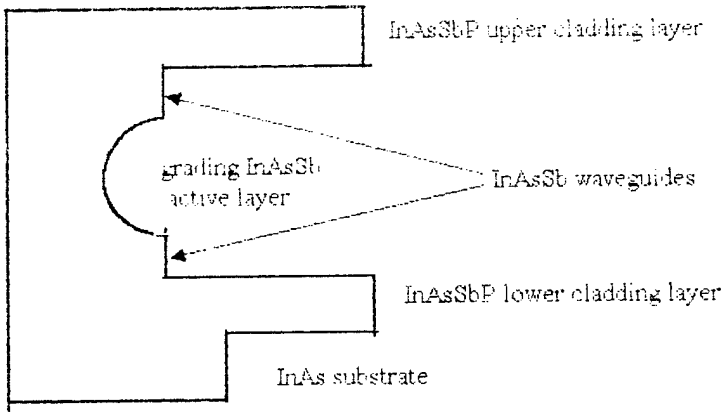

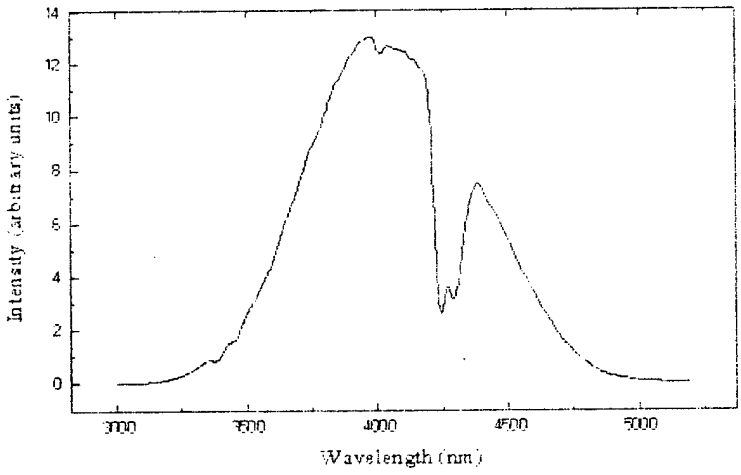

c) PL from separate confinement multiquantum well structure:

For the purpose of decreasing threshold current and increasing radiative efficiency, the SCH structure has been grown. The structure and PL spectra are shown below:

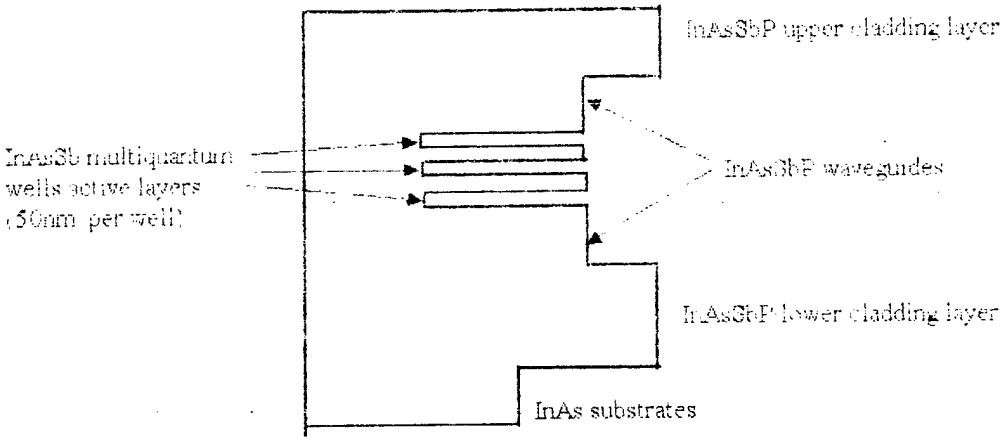

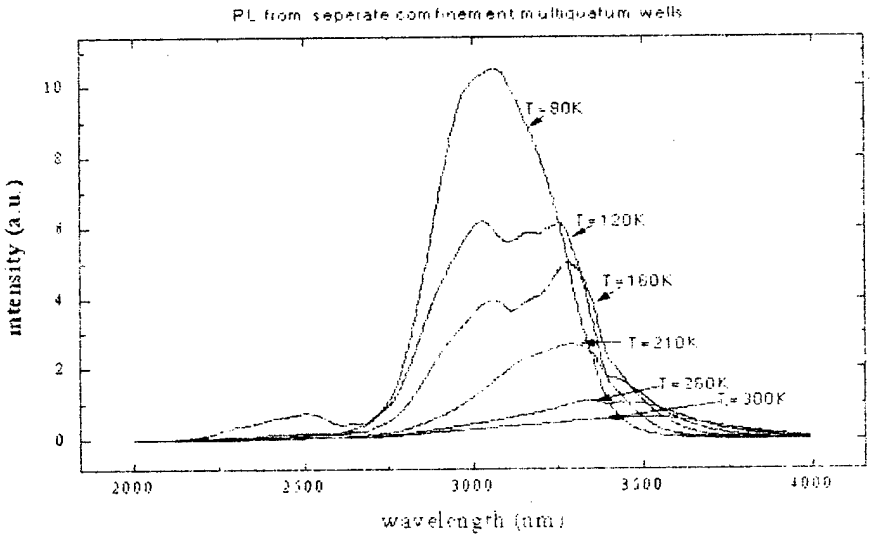

d) InALAsSb/InAsSb/InAlAsSb DH structure which can give higher cladding barriers

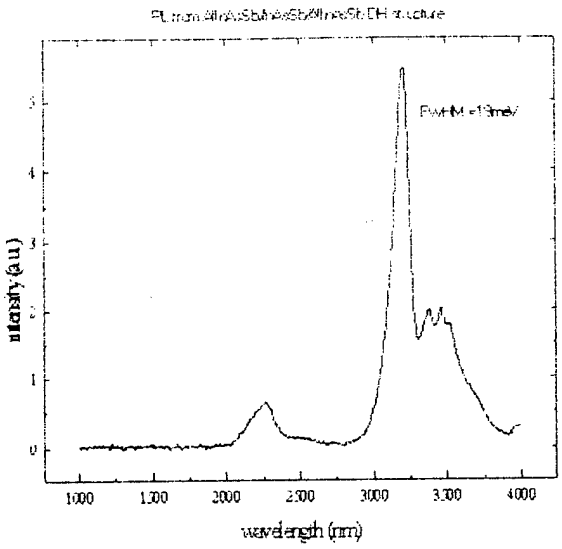

2.6 InAsSb/InAs(Sb)(P) strained layer MQW laser structures:

High power III-V compound semiconductor diode lasers emitting at the mid-infrared (3-5μm) are of practical interesting. InAsSb is a promising candidate for the active region of mid-infrared lasers, for it can easily cover 3-5μm region by adjusting the composition and moreover it is stable for growth and have a fair wide growth window.

One of the most wide used substrate for InAsSb based diode laser is InAs. For conventional DH laser structure. InAsSb/InAs structure suffer from mismatch between the epi-layers and the InAs substrate. While laser wavelength between 3-3.3μm at 77K, the mismatch between epi-layer and InAs substrate is between 0-0.4%, which is tolerable for laser application and as a matter of fact high performance DH laser diodes have been

fabricated in the 3 -3.3μm wavelength region which give high output power (680mW) and fairly high maximum operation temperature (220K). But if we want to push wavelength to longer region, the misfiting dislocation generated at InAs substrate and epi-layers will degrade the material quality and laser application. To avoid the above problem, InAsSb/InAs strained layer MQW active region has been used in both optical pumped and injected laser structure.

In this report, the study on InAs/InAsSb MQW grown by LP-MOCVD are presented by using high resolution x-ray spectra and photoluminenance spectra. Laser diodes with InAs/InAsSb active region have also been fabricated.

High quality InAs/InAsSb MQW structure has been grown by vertical stainless steel LP-MOCVD developed in EMCORE corporation. In order to have better PL performance, InAsSbP upper and lower cladding layers have been grown to sandwich the InAs/InAsSb MQW region.The detail structure are shown in the following figure 2..1.

Following the InAs buffer layer, 10 periods InAs/InAsSb MQWs with 50nm InAs barrier and 10nm InAsSb wells are grown between a InAsSbP lower cladding layer (~1μm) and a InAsSbP upper cladding layer (~0.6μm)

Fig.2.2 (b) shows the x-ray (004) diffraction pattern for a typical sample, which is measured by a four crystal x-ray diffractometer developed at Philips Research Laboratories. The broadening of the satellite peaks away from the 0th order indicates the fluctuation of the MQW periods. The InAsSbP cladding layer peak are overlapped with the 0th satellite peak, which is responsible for the broadening of the peak. The strong asymmetry observed comes from the strain and the possible interfacial layers between barriers and wells. Fig.2.2 (a) shows the simulated pattern with the bi-layer mode, that is the interface between InAs and InAsSb are assumed to be sharp without any interfacial layers.The obvious difference between this simulated result and the measured one, (b), is that the 3rd order satellite peak is missing in the simulated result but exists in the measured one, which suggests existence of the interfacial layers. The flow sequence of the sources during the growth of the MQW is shown in Fig.2.3. From InAs to InAsSb layer, 5 second interruption is used to pump out the AsH_3 for InAsSb growth needs much less AsH_3 than that is needed for InAs growth. From InAsSb to InAs layer, 3 second interruption is used to

Fig 2.1 The structure of InAsSb/InAs MQW structure

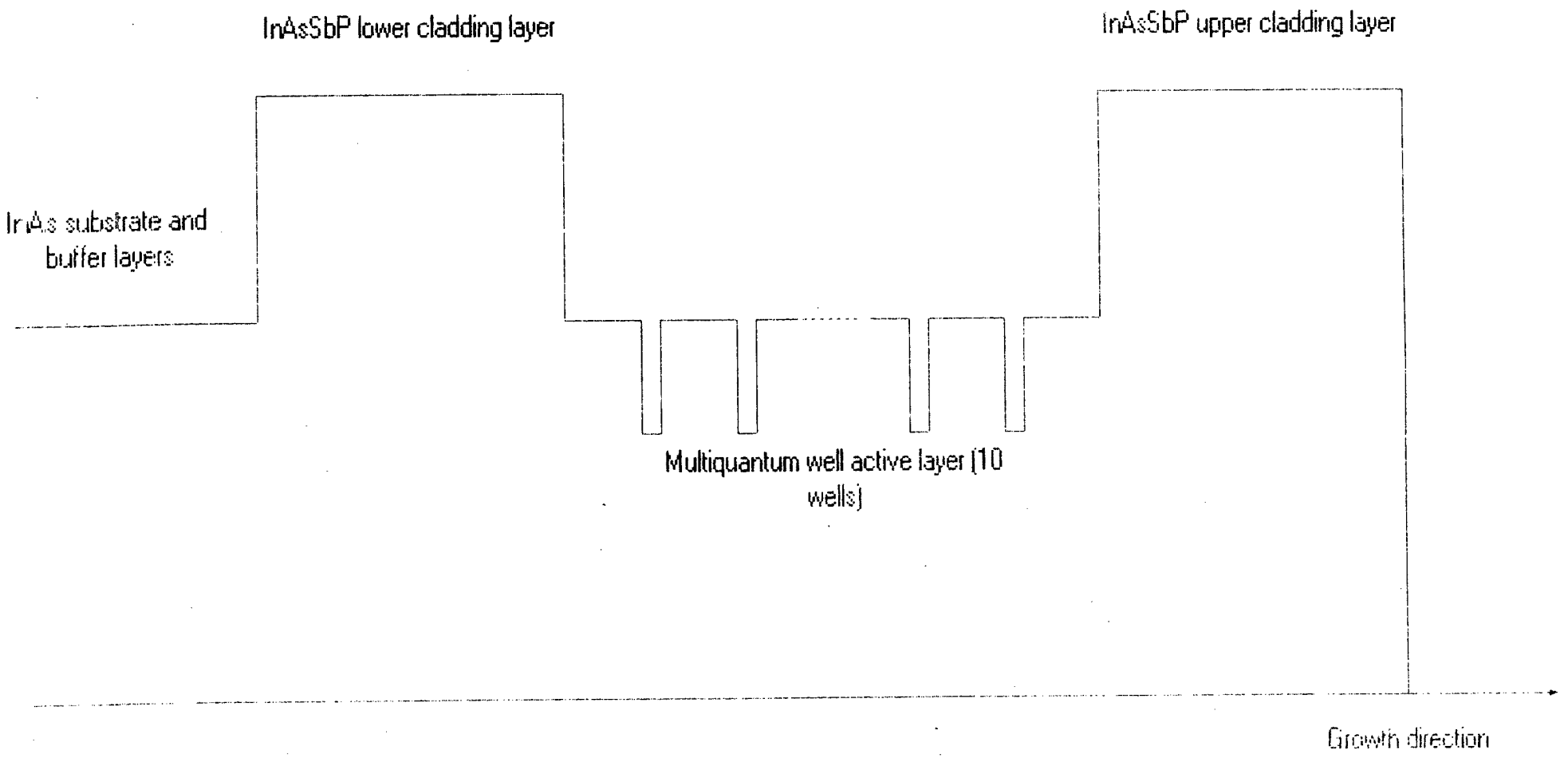

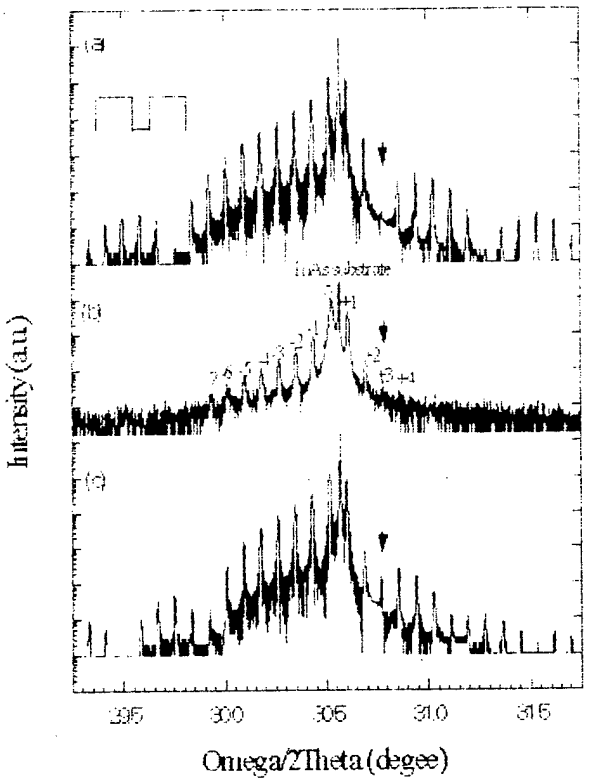

Fig 2.2 x-ray spectrum from InAsSb/InAs MQWs

get rid of the possible memory effect of Sb and In for TMIn and TMSb have relative larger size than that of hydrides and are not easy to purge out of chamber. The purpose of continuous flow of 5% AsH_3 is that it garantine the composition of interfacial layers will be between well and barrier composition so that we can suggest that the interfacial layer shape is something like that in Fig2..2 (c). From the simulated x-ray pattern of (c), we can see that after adding the interfacial layers the missed 3rd order satellite peak appears, which indicated this mode is closer to the real case. From simulation we get that the well thickness is 9.2nm, the barrier thickness is 49.8nm and the interfacial layer thickness is 1.8nm and 0.5nm from InAsSb to InAs and from InAs to InAsSb respectively. The Sb composition in InAsSb layer is 11.7%.

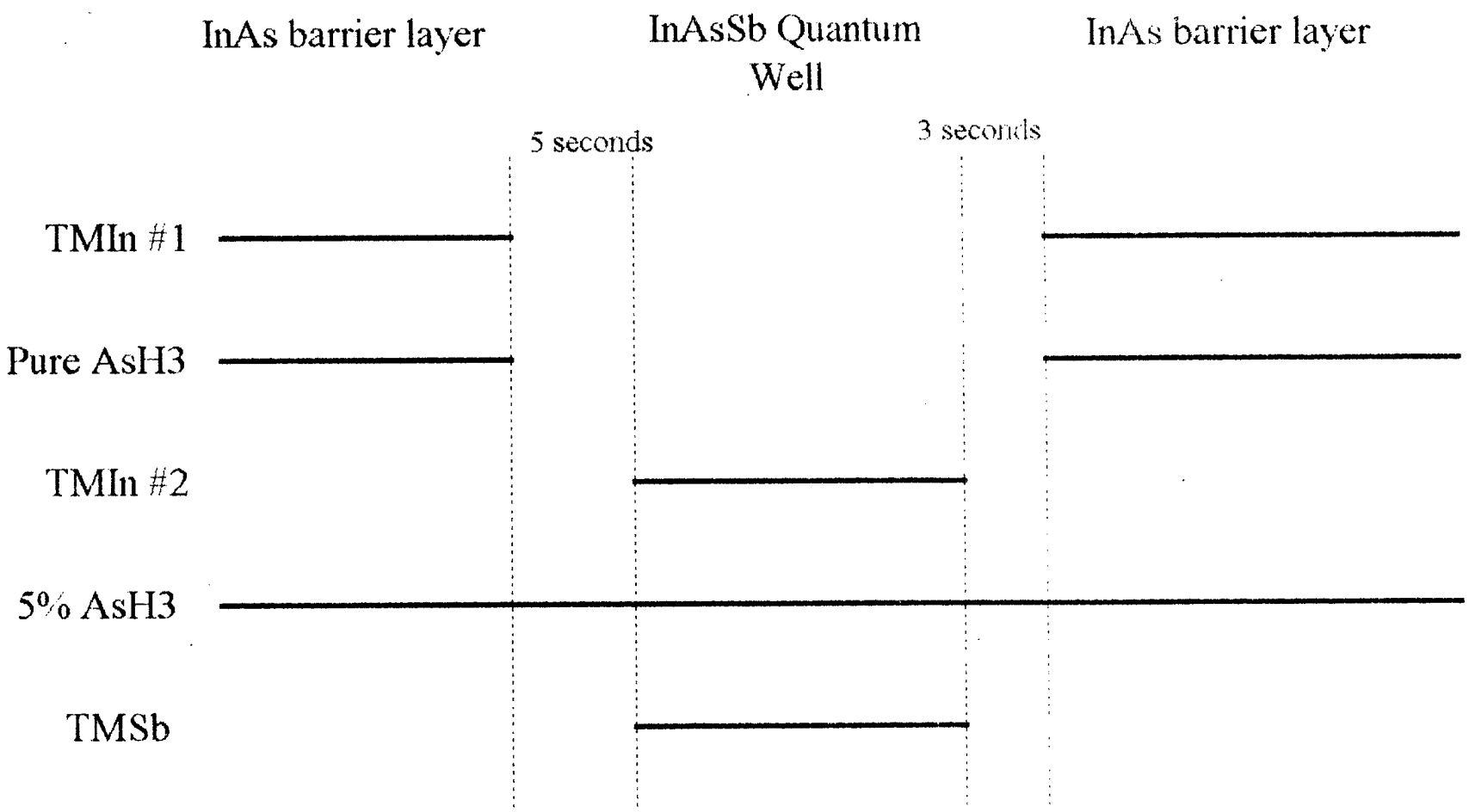

Fig. 2.3 The flow sequence of sources for the growth of InAsSb-InAs MQWs

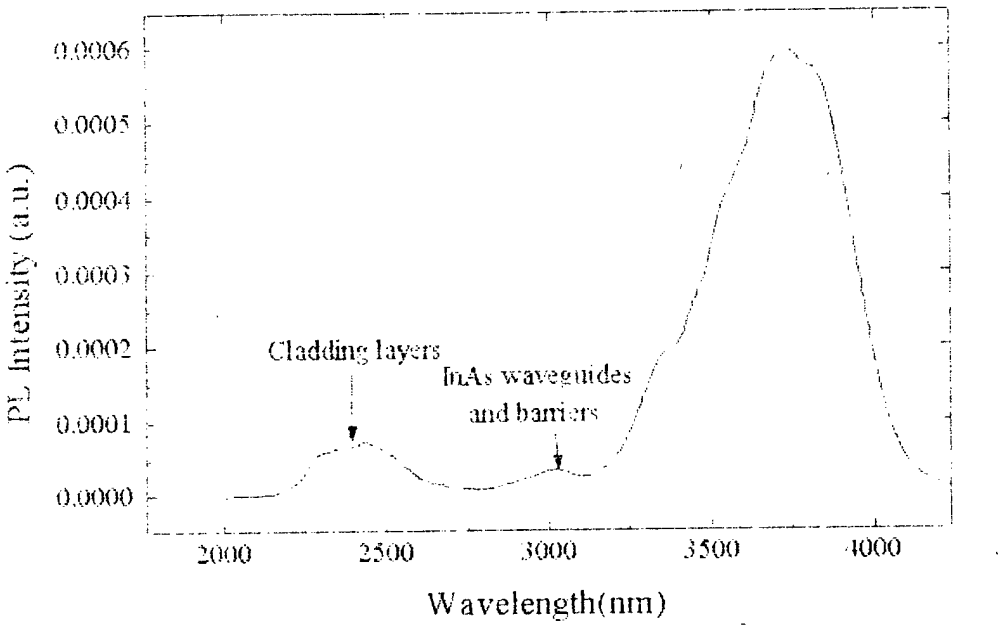

Fig. 2.4 The typical PL spectrum from InAsSb/InAs MQWs structures

Fig 2.4 is a typical PL spectrum at 77K from a sample. From Fig.2..5, which is α as function of temperature where we define α as the PL intensity ration between InAsSb wells and InAs barriers, we can see that carrier confinement dramatically improved with the decreasing of the bandgap of InAsSb well, which recommend that InAs/InAsSb MQW is more suitable for the laser with wavelength longer than 3.6μm. But for longer wavelength more Sb should be incomposed into InAsSb layer, the InAsSb material quality will be critical for laser application, for high Sb involved InAsSb layer is not easy to grow.

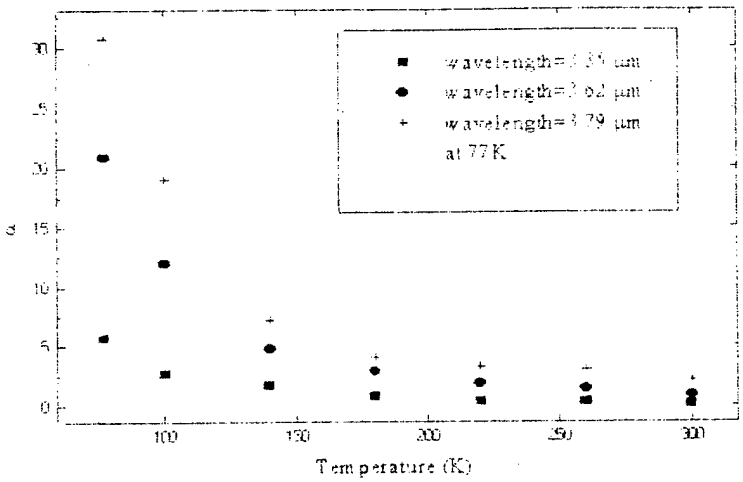

Fig. 2.5The PL intensity ratio, α, as a function of temeperature for samples with different wavelength

The critical thickness of InAsSb well is evaluated in the Fig.2.6 , where PL and x-ray measurement is applied

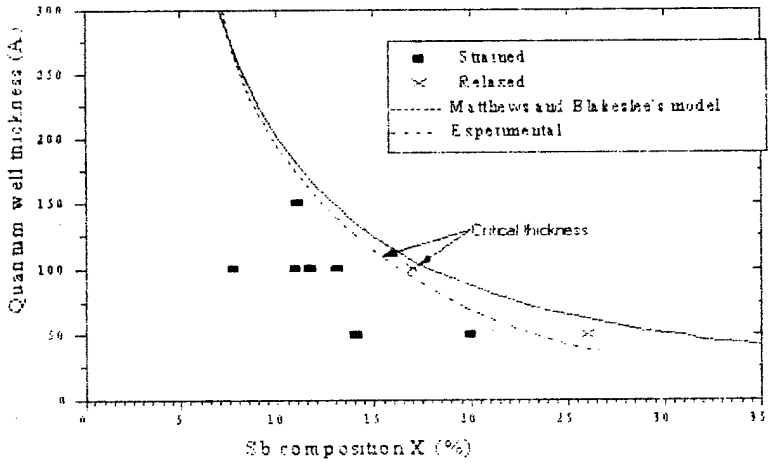

Fig 2.6 The critical thickness for InAsSb/InAs strained QWs.

The curve is the calculated critical thickness according to Matthew and Blakeslee's model. The black squares represents the InAs/InAsSb sample with fairly good x-ray and

PL spectra, while the cross represents the sample with broad x-ray satiate peaks and quenched PL spectrum indicating the release of the strains and large amount of misfiting dislocation generated which degrade the sample quality. The critical thickness evaluated from our data is shown with the dotted curve in the graph, whose value is lower than that given by the calculated one, which indicates again that the interface is not perfect and interfacial layer may exists.

CHAPTER 3

FABRICATION TECHNOLOGY AND PROCESSING OF LONGWAVELENGTH LASERS EMITTING AT 3.2μm

1. Introduction

The design structure of a SCH laser diode is to achieve both maximum carrier confinement and efficient optical confinement. The SCH lasers, as proposed in 1973 by Thompson and Kirby, consists of five layers such that the center composition step between the active layer and the waveguide layers gives an energy band discontinuity to confine injected carriers within the active layer, and the outer step in the refractive index between the waveguide and cladding layers confine the light within the optical cavity. Separate optical and electrical confinement ensures moderate beam divergence and optical power density at the laser mirror, while preserving fundamental transverse mode operation and low threshold current density for lasers with thin active layers. The preference of quantum well lasers offers (i) high differential gain to attain low threshold current density; (ii) small optical confinement factor, and (iii) a small variation of threshold current with temperature.

The light emitting area of a laser diode is confined by a stripe contact resistance of some width, W, in which most current will flow through the ohmic contact region. The stripe contacts are created by the combination of metallization and photolithographic techniques. The processing of longwavelength laser diodes follows the same traditional concepts of 808 nm InGaAsP/InGaP/GaAs lasers fabrication. The following section introduces the experimental studies and optimizations that were employed to the Sb-based material.

2. Growth of InAsSbP/InAsSb/InAs Structures

2.1. Introduction

The epitaxial layers for the Double Heterostructure (DH) and the Separate Confinement Heterostructure (SCH) of InAsSb/InAsSbP/InAs are grown by low-pressure metalorganic chemical vapor deposition (LP-MOCVD). The DH wafers consists of (100) n-InAs substrate (Te-doped, ~10^{18} c m^{-3}) and the following layers are grown: an n-type Sn-doped (~10^{18} c m^{-3}) InAsSbP lower confinement layer, an undoped InAsSb active layer (1μm), and a final p-type Zn-~10^{18} c m^{-3} InAsSbP upper confinement layer with a p-doped InAs (~10^{18} c m^{-3}) cap layer. Figure 2.1 shows the cross-section of a DH laser structure. Figure 2.2 shows the cross-section and band structure of a SCH laser, which were grown on n-InAs (100) substrates by LP-MOCVD. The SCH layers were grown in the following order: n-InAs buffer, a n-InAsSb cladding layer, an InAsSbP waveguide layer with an undoped InAsSb ternary active region, and a final layer of InAsSbP waveguide layer. In general, the design and fabrication of SCH laser structures offers a quantitative number of interesting characteristics. The most important characteristic includes: (1) the low threshold current density, (2) the small variation of the threshold current with temperature, and (3) the ability to tune of a particular wavelength.

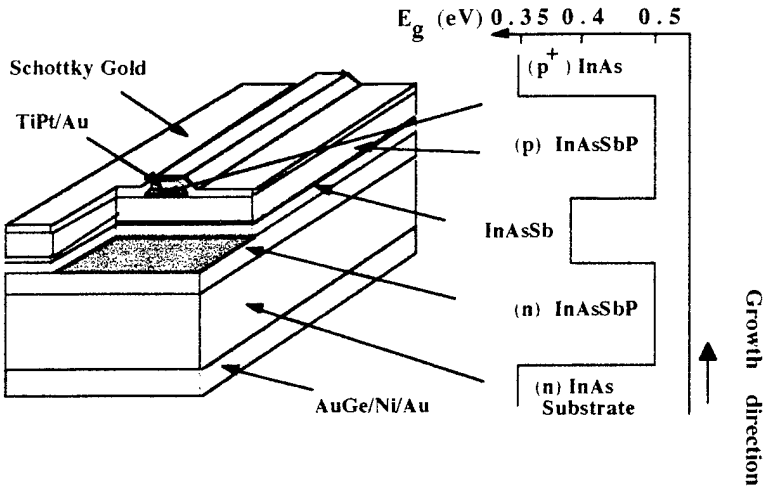

Figure 2.1 Cross-section of a Double Heterostructure

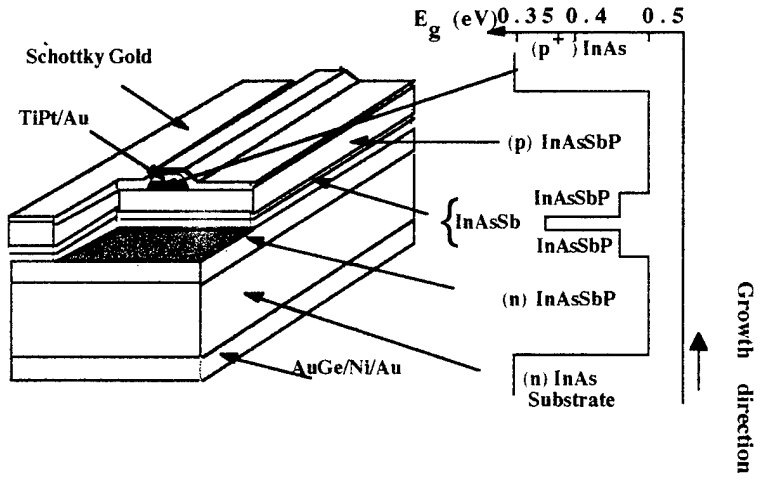

Figure 2.2 Cross-section of a Separate Confinement Heterostructure

3. Fabrication of InSb-based Materials

3.1. Introduction

The technology of lasers is made of several components which utilizes photolithography technology to metallurgical technology. The essence of every laser processing consists of a standard procedure that must be followed and controlled extensively to produce laser diodes of high performance. One of the crucial stages after the epitaxial growth is the preparation of the wafer for fabrication as well as etching, metallization, annealing, and thinning of InAs. This report discusses the experimental studies on InAs-based material and continuing efforts are being made to optimize the processing of these 3.2 μm lasers.

a. Surface Preparation of InAs (100)

A very important step in the fabrication InAsSbP/InAs laser structure is the initial surface cleaning of InAs. The strong dependence between the metal film and wafer condition should be known. The desired wafer surface before metallization or even before epitaxial growth must be smooth, mirror-like, without epitaxial pits, oxide and carbon free. The chemical processing of InAs is very difficult because of its small bandgap, reactivity, and limited solubility of the reaction products. Investigations of InAs, especially surface preparation, has received much less attention compared, for instance, to GaAs. However, due to the significant interest in device application, increasing effort has been made to address surface preparation for InAs. Thus far, InAs substrate preparations have involved common methods similar to those used for cleaning GaAs or InP substrates. The most common used surface cleaning consists of hot tricholorethylene, acetone, methanol, and deionized water rinse followed by a 1% hydrofluoric acid rinse. Following the InAs preparation, the wafers are then prepared for processing which constitutes

photolithography, metallization of contacts, chemical etching, lapping, cleaving, and die bonding.

b. Photolithography

Photolithographic techniques are widely used in transferring device patterns onto semiconductor materials with a high degree of accuracy. The photolithographic processing revolves around several steps, regardless of the particular photoresist application being used or the layer to which it is being applied. The steps involved in photolithography will be discussed briefly in the following steps.

1) Photoresist Application: Photoresist is a chemical substance containing a light-sensitive material in suspension in a solvent. The light-sensitive material is selected so that it responds to a intense blue-violet produced by a mercury arc lamp, but does not respond to the red or yellow light commonly in use in darkrooms or photoresist application areas. Photoresist comes in two distinct types:

i. Positive resist: The light from the exposure step increases the solubility of the resist in the developing solution, by depolymerizing the resin.

ii. Negative resist: The light from the exposure step causes polymerization to occur in the resist, reducing the solubility in the developing solution. This type of resist may be thought of as light-hardened.

The advantage of using AZ-5200 series photoresist is that it can be made to image reverse to a negative tone via a simple post-exposure bake (PEB) process as well as other features as:

Near vertical profiles to give accurate pattern transfer in plasma and reactive ion etching.

Excellent photospeed in near-UV (365 nm-405 nm) and mid-UV (300nm-350nm)

Wide process latitude

Excellent resolution in both metal-ion free and inorganic developers.

High thermal stability (~150C) to maintain profile quality during plasma etching or chemical etching and ion implant process

Sub-micron resolution capability

The application of photoresist consists of introducing small amounts of AZ5214 resist to the InAs wafer surface through a 0.2 μm filter to remove any form of polymerized particles. To applied the resist uniformly onto the semiconductor surface, the samples are placed onto a vacuum chuck that is held down by vacuum which it is then rapidly accelerated to 3000 rpm for 25 seconds to acquire a resist thickness of 1.7 μm for 100 μm and 50 μm windows. If narrower window are required, for instance, 1 μm to 20 μm linewidth, then the photoresist thickness must be reduced from 1.7 μm to 1.2 μm or less. This is accomplish by accelerating the spinner to 5000 rpm or 6000 rpm. The thickness of the resist coating depends upon the viscosity of the resist and the rate of acceleration of the spinner. Control over the thickness and uniformity of the resist is very important in controlling the pattern dimension during exposure as well as during developing. Efforts are being made to keep the semiconductor devices clean and free from dust during this stage of the processing.

2) Soft Bake: Soft baking is necessary to prevent solvent trapping and possible bubbling or peeling of the resist. Resist adhesion to the substrate is improved with increased drying time. This is usually carried out on a hot chuck or in a conventional oven which heats the substrate and the resist film to a temperature of about 90 °C. Improper baking can result in hardening of the resist surface prior to the removal of all residual

solvent which can result in pin holes and poor uniformity of the imaged dimensions and improper lift-off profiles.

3) Alignment and Exposure: Alignment and Exposure are the most critical and significant part of the photolithographic process. The exposure equipment used in this process is called a mask aligner. This machine aligns the photoresist-coated substrate and the mask, and exposes the photoresist film to ultra-violet light through the mask. The mask contains the pattern to be transferred to the substrate, in this case, a 100 μm-wide stripe. The exposure time ranges from 10 - 15 seconds and is dependent on the age of the photoresist and the excitation lamp. Actual exposure energies required will depend on film thickness, SoftBake conditions, spectral output of the exposure tool, and developing conditions.

4) Development: The development of photoresist is accomplished by immersing the wafer in a developer solution for a predetermined amount of time. This developer dissolves the exposed areas of the photoresist, while the unexposed areas remain insoluble and remain on the substrate. This process of replication transfers the photomask pattern onto the semiconductor substrate.

5) Post-Baking: Postbaking will generally improve image stability and adhesion as well as plasma and chemical resistance. The extent of Postbaking, if required, will depend on many other process parameters and should be determined by the user. The heat treatment is done by a baking at temperatures ranging from 100 °C to 120 °C for 30 minutes or a few seconds when using a hotplate. The post baking conditions are very critical to obtain lift-off profiles such as shown in Figure 3.1. If improper exposure or Postbaking conditions are not met, the mask replication will provide vertical profiles rather than lift-off profiles.

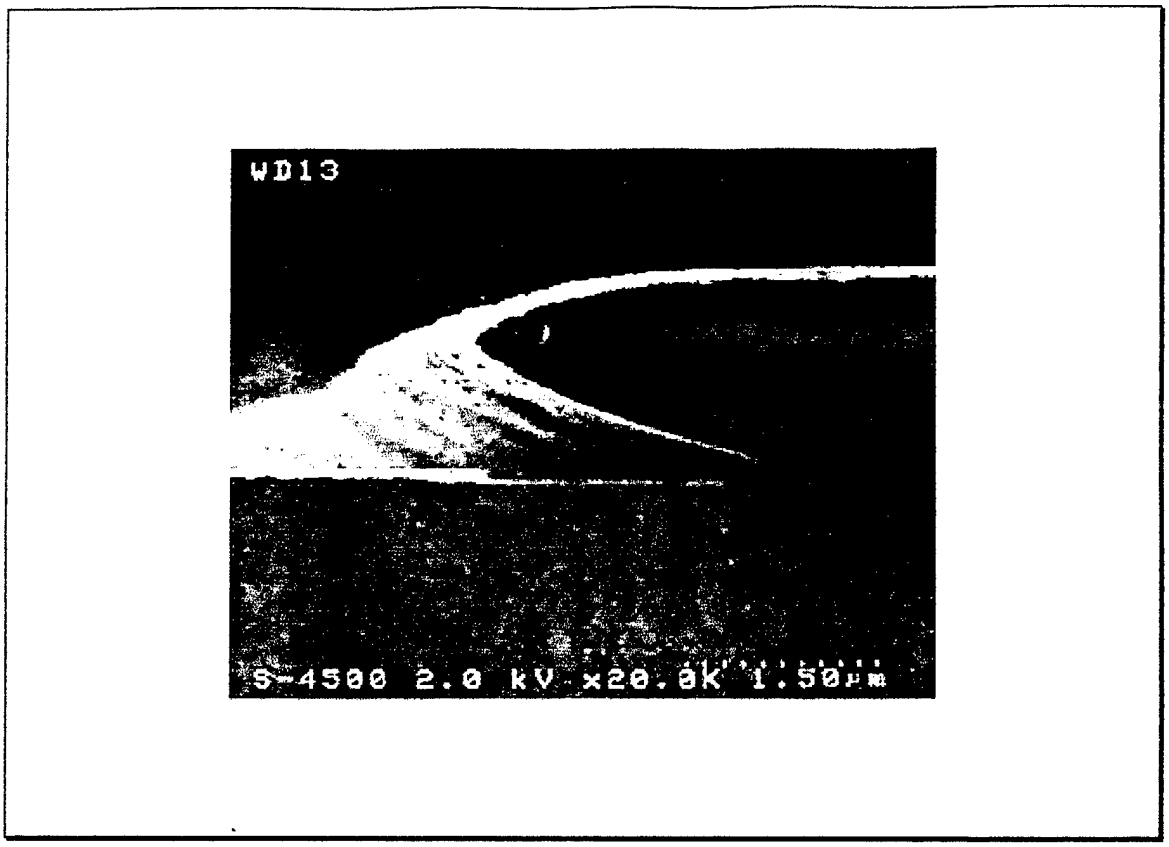

Figure 3.1. SEM cross-section of a lift-off profile necessary when depositing TiPt/Au metallization system.

c. Metallization of Ohmic contacts for p-InAs-base material

The successful operation of optoelectronic devices is determined to a large extent by the quality of ohmic contacts. In the past, most of the ohmic contact studies have been focused mainly on GaAs, InP, and Si because these semiconductors have been used in

industry. Contacts on n- and p-InAs have been studied less in spite of its potential for applications, such as in photodetectors and lasers. To date, there has been little investigation of the characteristics and the effects of interdiffusion between metal and InAs semiconductor. In the case of GaAs semiconductor, the primary consideration in the choice of an ohmic metallization system is: low contact resistance, thermal stability, good morphology, good adhesion to and shallow penetration of the contact layer(s) into the semiconductor and the resistance to wet chemical processing. N - and p - InAs ohmic contacts have been studied by few author's. However, these specific studies are mostly concentrated on the electrical properties of ohmic and Schottky contact resistance and the interfacial micro-structural characteristics of various metal films on InAs by using Auger electron spectroscopy, transmission line model (TLM), Rutherford backscattering spectrometry (RBS), and X-ray diffraction. In our case, we will study the effects of specific ohmic resistance for p- and n- InAs semiconductor by evaporating TiPt/Au and AuGe/Ni/Au, respectively. Specific studies done by others will not be discussed in detail in this report.

After obtaining lift-off profiles, the metallization of contacts are deposited. The metal deposition of TiPt/Au is accomplished by inserting the prepared wafers into a electron-beam evaporator under high vacuum. The pressure in the chamber is reduced to the range of about $2x10^{-6}$ to 10^{-8} torr. This ensures that virtually all the evaporant flux will reach the semiconductor surface, and to prevent any undesirable chemical reactions between the evaporant molecules and the residual gases in the vacuum chamber. The evaporated material is placed in a water cooled crucible in which a focused beam with very high power density is directed at the surface of the material. This makes a small region of the material to heat up to a very high temperature enough to be vaporize. The evaporated molecules that hit the semiconductor surface will condense there and form a thin-film coating. The thickness of the deposited film can be monitored during the evaporation

process by a quartz crystal film thickness monitor that is situated about 35 cm above the water-cooled crucible. As the film thickness builds up on the exposed face of the quartz crystal, it increases the net mass of the crystal. When the required film deposition has been reached, the evaporant material can be shut off automatically by means of a shutter that is placed in front of the evaporation source. Immediately, following the evaporation, the wafers are inserted into suitable solvents as acetone to remove unwanted metallization and maintaining 100 μm metal stripe contacts on the InAs surface. As shown in Figure 3.2, the InAs wafers are composed of 100 μm TiPt/Au stripe contact with 300 μm spacing.

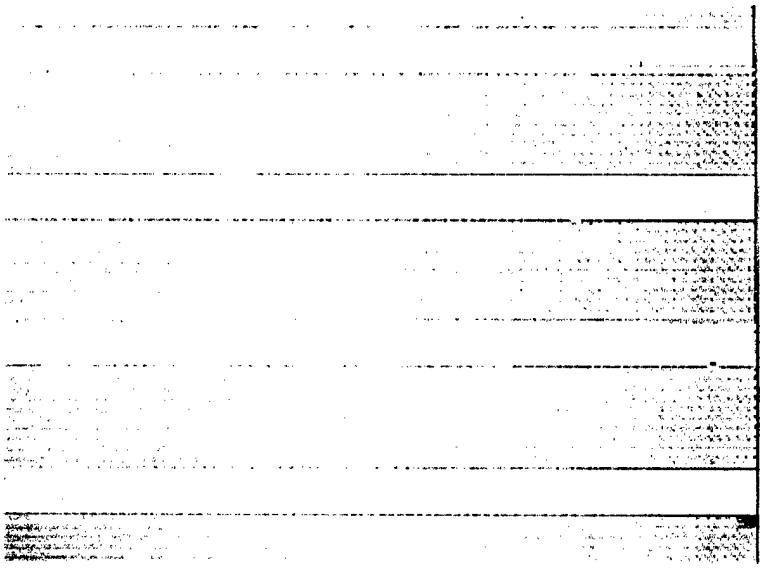

Figure 3.2. Top view of 100 μm stripe metal contact on InAsSbP/InAsSb/InAs laser structure by utilizing lift-off technique (x4 magnification).

d. Etching InAs-based materials

An important step in the fabrication of optoelectronic devices is the removal of one or more semiconductor material layers, in order to make electrical contacts, isolate individual layers in a structure, or even to remove excess semiconductor materials. Large amount of studies devoted to the etching of GaAs, InP, and Si has been reported over the years. With respect to InAs, little work has been done on the chemistry etching over the years, until now. Many etching methods have been proposed to achieve smooth, etch pit free, and mirror-like surfaces; however, most of them give contradictory results.

Experimental Studies and Results on InAs

We have studied several chemical etchants listed in Table 1 in order to determine a suitable, reproducible chemical process to form uniform ridge structures. To compare efficiency and surface morphology of each studied etchant, a 1mm by 1mm n-InAs substrate was used for etching experiments. Table 1 is a list of etching solutions that have used to experimentally etched or polish the InAs surface prior to growth films and chemically etch InAs to isolate individual layers. Whether it's InAs, GaAs, or any III-V semiconductor

Table 1

	Solution	ratio	surface
A	Br_2: Methanol	5:1000	roughness, fast etchant, 5-10%trench
B	$HF:HNO_3:CH_3$-COOH	1:10:30	uneven etch
C	$HSO_4:H_2O_2:H_2O$	1:1:20	roughness reduce

materials, there are general rules which are characteristics of each etching mechanisms that are useful in determining the dominant etching mechanisms.

Diffusion-limited etching -

a. Etch rate (etch depth) is proportional to the square root of the etching time.
b. Etch rate increases with stirring or agitation of the liquid etching.
c. Etch rate is relatively insensitive to temperature variations.
d. Etching is more isotropic with respect to crystal orientation.

Reaction-rate limited etching -

a. Etch rate (etch depth) is linearly proportional with the etching time.
b. Etch rate is unaffected by stirring or agitation of the liquid etchant.
c. Etch rate changes with temperature.
d. Slight changes in relative proportions of etchant components can result in large changes in etch rate.
e. Etchant gives faceted surface structure characteristic of the crystal material properties with flat bottomed opening.

All experimental samples were immersed into each etchant solution (A, B, or C) faced-up for two minutes at room temperature. Among the three main etchants outlined in

Table 1, the composed HSO_4:H_2O_2:H_2O etchant resulted in mirror like surface, less amount of roughness, and uniform across the sample. However, decreasing the proportionality of H_2O effects the etching rate as well as the uniformity of the InAs surface. A typical profile of an etching step of a 100 μm mask edged is shown in Figure 3.3. The etching depth in Figure 3.3 is measured as the difference between the surface level of the unetched region and the flat level etched area. The gain-guided laser for InAsSbP/InAsSb/InAs material is produced by etching a portion of the p-InAs cap layer. The thickness of the cap is layer estimated between 0.0900 μm - to 0.100 μm. To completely remove the InAs cap layer between the 100 μm stripes, a 0.120 μm InAs etch layer is removed utilizing solution C. In using method A or B as a etchant for InAs, leads to enhanced trench (5-10%) near the boundary of the etched and unetched area. Furthermore, these solutions are uncontrollable and the etching rate changes as the solution ages with time.

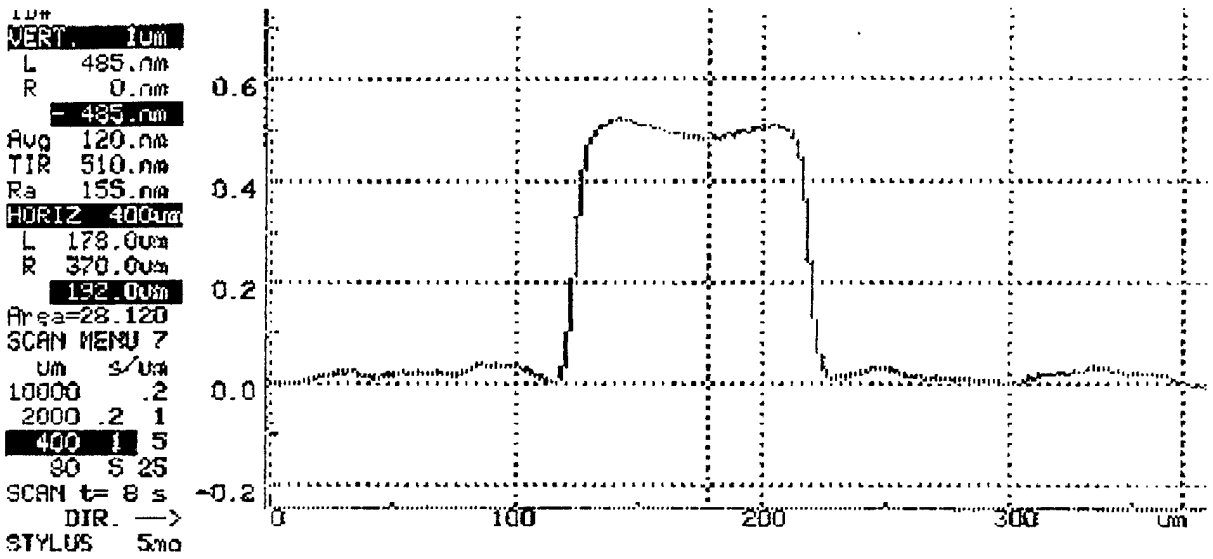

Figure 3.3. Alpha step profile of 1.20 μm InAs etch utilizing H_2SO_4:H_2O_2:H_2O solution.

Experiments are being conducted to utilize the SiO2 technology and produce ridgewaveguide lasers rather than gain-guided lasers. The ridgewaveguide lasers are being study to be provide electrical and optical confinements of the current. Stripe widths of 50 μm and 10 μm mesas with 10μm and 5 μm openings for the SiO_2 are used, respectively. Several wafers were used in this experiments consisting of wafer #92 and #99 with 10 μm mesa and 5 μm window for passivation. Wafer #94 and #1071 carried 50 μm mesa etch with 10 μm opening for the SiO_2 mask. The 50 μm X 300 μm mask was used as the contact pad which will eliminate further damage on the stripe during wire bonding as shown Figure 3.4.

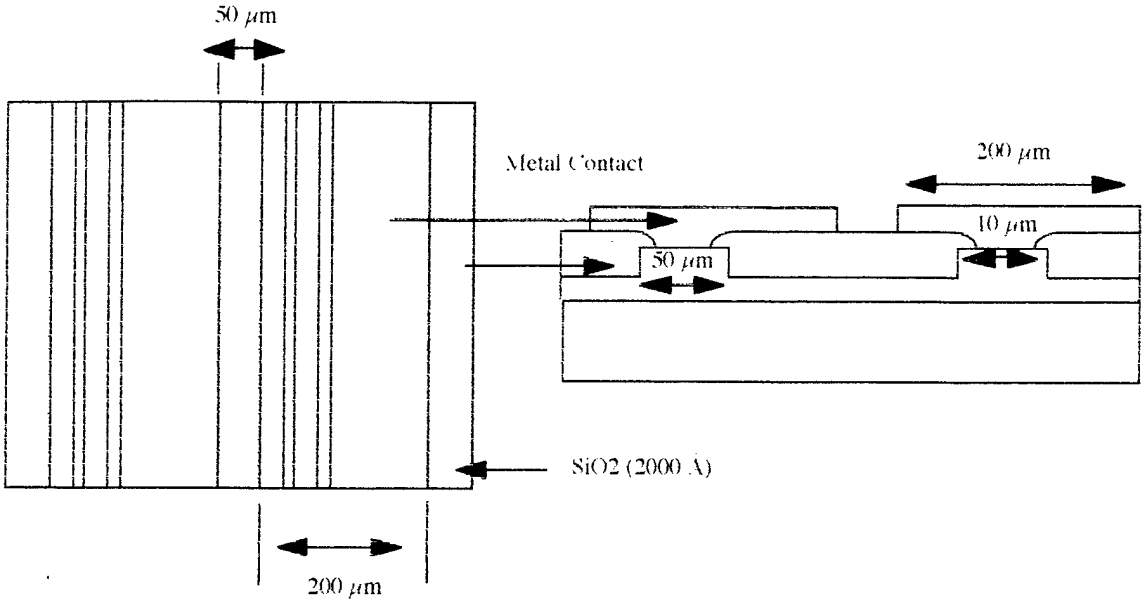

Figure 3.4. Top view and cross-section view of a ridgewaveguide (RW) laser structure.

The 50 μm and 10 μm resist linewidth resulted in sharp resolution edges by photolithography. Typically, in removing the InAs cap layer between the stripes, an etch of 0.120 μm is removed by utilizing H_2O_2: H_2SO_4:H_2O (1:1:20) for at least 40 seconds. However, in order to reduce the current leakage than we have been observing in measurments, it is necessary to remove a large portion of the cladding layer at least 0.6 μm to 0.8 μm. Such that the structures will be more of a ridge waveguide laser, where it can provide a better current and optical confinement. In removing a total layer of 0.6 μm of the cladding layer, resulted in undercutting of the InAs cap layer. This undercutting for narrow stripes such as #92 and #99 resulted in 5 μm or less instead of 10 μm. Following the a deep etch, the wafers were inserted in the e-beam evaporator for a 2000 Å thickness of SiO_2. A 10 μm and a 5 μm window were open for the 50 and 10 μm mesas, respectively. To acquire a 5 μm or a 10 μm opening, a dark field mask must be used. However, using the dark field in our case, it is very difficult to properly align the SiO2

pattern directly onto the wafer pattern. Therefore, a light field mask was used in these experiments. By utilizing this method, brings additional concerns with the removal of the SiO_2 on the 5 μm and 10 μm openings. This concern consists of undercut of the SiO_2 when using a high diluted HF or BHF solution. To avoid this, a new set of mask is required for the longwavlength lasers. Following a SiO_2 etch, TiPt/Au is deposited onto the wafer area in order to provide a 200 μm contact pad.

e. Lapping and Polishing of InAs

In the fabrication of lasers, it is necessary to thin the substrate to a thickness of 100 - 110 μm. No studies have been done on this subject to the best of our knowledge. In our preliminary studies on lapping/polishing of InAs, we have found a suitable processing technique to polish n-InAs substrate as thin as 120 μm.

Experimental Studies on Lapping/Polishing

Wafers of n-type (100) InAs were used in these experiments. After cleaning the substrate with cleaning procedures outline in section *"Surface Preparation of InAs (100)"*, the wafers were prepared for lapping and polishing processing. Unlike GaAs substrates, this type of semiconductor requires special care.

The technique used for the thinning of InAs substrates is called lapping/polishing. The primary factor in lapping/polishing of n-InAs substrate is to make the cleavage of laser diodes or bars more feasible, since the initial thickness of InAs substrates are generally 300 to 350 μm-thick. Generally in the fabrication of InGaAsP/InGaP/GaAs lasers, the wafers are covered with a protective layer of photoresist on the p^+- side surface to prevent any buildup of contaminants that occurs during this stage of processing. The same concept is applied to the InAsSbP/InAs lasers. After depositing a layer of photoresist, the wafer are

bonded p-side down onto a glass substrate (83mm diameter x 6mm nominal thickness) by an excess of wax. All excess wax are scraped away from around the edges of the wafer and the glass substrate. It is of the utmost importance for the operation of lapping/polishing to ensure that all traces of exposed wax have been removed from the wafer/glass substrate assembly. There is the risk, once lapping/polishing has begun, any remaining wax might gather together to form a wax ball which could badly damage the surface of the wafer if it were to pass between the wafer and the surface of the glass lapping/polishing plate.

The glass substrate along with the bonded wafers are then mounted onto a vacuum jig apparatus. The jig apparatus has the facility of increasing or decreasing the amount of load to be applied when lapping/polishing. The jig apparatus is then placed onto a glass lapping plate; however, before placing the jig and wafer/glass substrate assembly on the glass lapping plate, ensure that the surface of the plate is free from accumulation of dried aluminum oxide abrasive powder. The simplest way to remove this is to spray or rinse the surface of the plate with deionized water.

Upon placing the jig onto a glass lapping plate, the plate is rotated slowly (5 rpm) using the speed control knob so that the jig describes ten complete revolutions. The purpose of this is to thinned down all the wafers evenly. The lapping procedure begins by setting the rotational glass plate to 5 rpm to lap the entire InAs substrate surface uniformly and to adjust the jig apparatus at low pressure. In order lap the InAs substrate, a 3 μm (abrasive size) solution of aluminum oxide abrasive powder is used. The lapping speed can then be increased to 30 rpm, and the jig pressure can be increased slightly to obtain a lapping rate of 5-10 μm/min. The lapped wafers are subjected to a visual and thickness examination to ensure that a satisfactory lapped have been achieved. This inspection can be made every 5 or 10 minutes. Once the lapped wafers reaches a thickness of 150 μm, the polishing stage is then proceeded by replacing the aluminum oxide abrasive powder from

3.0 μm to 1.0 μm granite and replacing the lapping glass plate with a polishing cloth plate. The polishing stage is to further reduce the InAs substrate thickness down to 120 μm, and to obtain a final mirror surface. Before moving on to the polishing stage of the process, it is of the utmost importance to ensure that all traces of 3 μm abrasive have been removed from the wafer/glass substrate assembly, as this might cause considerable surface damage during polishing. A suitable method of achieving this is to wipe the entire glass plate with trichloroethylene or alcohol. As before, adjust the variable pressure jig to the desired setting and mount the jig assembly onto the lapping/polishing machine.

The polishing process is also sensitive to both the polishing rate and pressure applied to the substrate. Excessive pressure or a high polishing rate will cause damage to the InAs in the form of dislocations which may propagate into the active region of the laser device during operation and cause premature failure. Several tests have been performed to find an appropriate setting to eliminate these defects. The polishing speed used for InAs is 20 rpm to 15 rpm with a jig pressure relative to a polishing rate of 0.5μm to 10 μm/min. Further reduction in speed and jig pressure are sometimes necessary when the thickness is about 120 μm. Figure 3.5 is an example of a polished 110 μm n^+- InAs substrate.

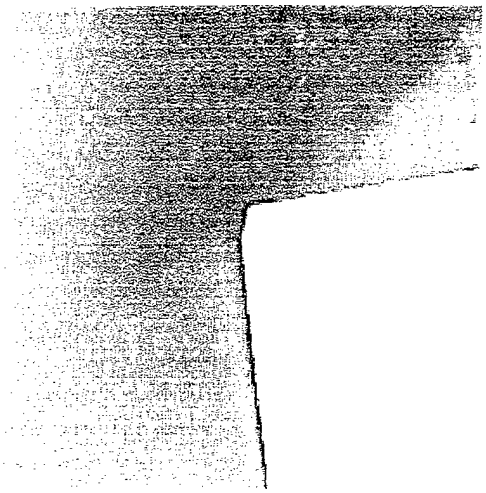

Figure 3.5. InAs substrate surface after lapping polishing with a thickness of 120 μm.

f. Annealing of p- and n- InAs contacts

Upon polishing the InAs substrate to the desired thickness, the wafers are prepared for the last deposition of metallization to the n-type InAs substrate. As indicated earlier, the deposition of multi-layer contacts onto a semiconductor is to form a low resistivity contacts between the p- and n- side of the semiconductor, to improve the wettability of the surface, and to provide better adherent to the bonding of indium heatsinks. In the case of n-InAs contact, AuGe/Ni/Au was used in our experiments and applied to the InAsSbP/InAsSb/InAs laser structures. The incorporation of nickel alloy to the AuGe and Au is to enhance the diffusion of germanium and limit the amount of gold diffusion into the lattice.

In order to achieve low contacts to the p- and n- side, heat treatments of the contacts are necessary. In our experimental studies of annealing to Zn and Sn doped InAs layers, heat treatments were carried out by means of open tube furnace under controlled forming

gas of 10 % H_2-N_2 ambient at temperatures between 250 and 400 C and duration of 2 - 3 minutes. The proximity heating approach was used to prevent substrate decomposition by placing the InAs samples with the metallized side up for the p-contacts and metallized side down for the n-contacts onto a silicon wafer. The electrical characterization involved measurements of current-voltage (I-V) and specific contact resistance by means of linear transmission method (TLM). Minimum values of 0.20 (and 0.36 (were obtained for these InAsSbP/InAsSb/InAs lasers at 77 K and 300 K, respectively. Heating the samples to temperatures higher than 350 C can reduce the influence of the doping level on the contact resistivity, and obtain decomposition of the metal film. In producing electrical contacts for any type of optoelectronic device, particularly in high power lasers, it is very important that the metal film is completely annealed and adhered to the semiconductor surface. Figure 3.6 (a) is an example of a poor metal adhesion following a low temperature annealing from a InAsSb/InAsSbP/InAs diode laser, whereas Figure 3.6 (b) consists of Ti/Pt/Au metal contact properly annealed to the InAs semiconductor surface. In fabricating good quality metal contacts, two factors are important: (1) the semiconductor surface must be properly cleaned prior to metal deposition, and (2) the annealing conditions should be carefully investigated and optimized.

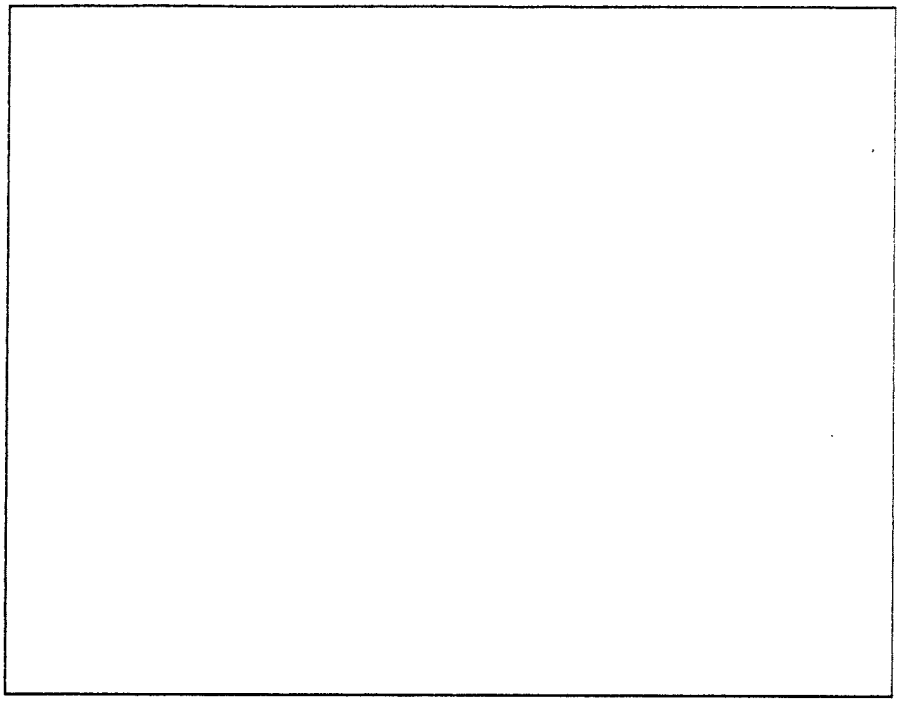

(a)

Figure 3.6. (a) Improper metal adhesion to the InAs semiconductor after contact annealing.

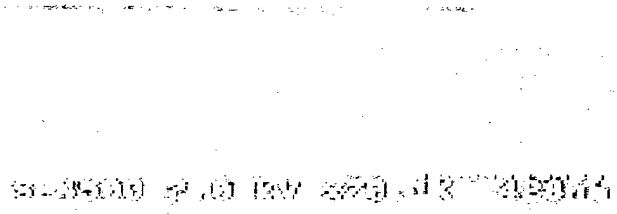

(b)

Figure 3.6. (b) Good metal adhesion to the semiconductor surface after annealing of 300 °C (2.0V, 70K magnification).

g. Post-Processing

The post-processing of InAsSbP/InAs wafers includes cleaving, die bonding, and wire bonding. The technology being applied after post-processing for these type of lasers are critical to device performance. As in the case of InGaAsP/GaAs lasers, the post-processing technology an amount of investigation and optimization have been performed to reliable high power devices. The same type of studies that were investigated in the 808 nm lasers are being applied to the 3.2 μm InAsSbP/InAs lasers.

(i) Cleaving of InAs lasers

A semiconductor laser diode consist of a stripe contact of width, W, and two cleaved mirrors of cavity length, L. These cleaved mirrors are formed by scribing lines at the edge of the laser wafer (perpendicular to the stripe contacts) with a diamond tip scriber system. Once the scribe lines are induced, a slight pressure is applied to the wafer causing the semiconductor crystal to cleave along its cleavage plane.

(ii) Die bonding of InAsSbP/InAs lasers

The bonding of laser diodes is very important for high power operation. In the case of InAs laser, the thermal conductance between the diode and the heatsinks is considered more important than high power operation at this time. Since these lasers are normally recycled between 77K and room temperature, the mechanical adhesion between InAs and the indium layer is important. The removal of excess heat from a laser device is accomplished by mounting a laser die onto a indium coated copper heatsink under ambient forming gas (10% H_2:N_2) as shown in Figure 3.7.

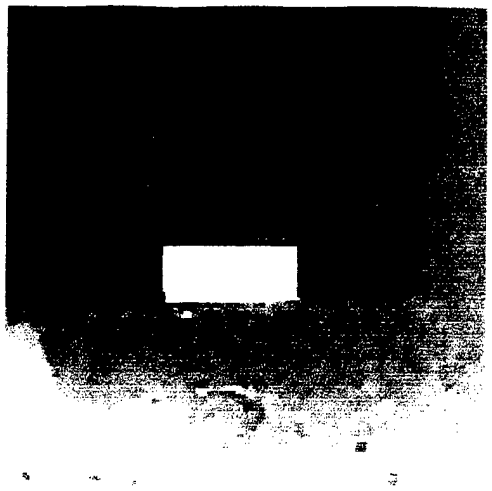

Figure 3.7. Laser diode bonded on indium copper heatsink

(iii) Wire bonding

The method used to interconnect the laser contact to the ceramic package is done by Au wire bond. In Au wire bonding, a spool of fine Au wire (about 1 mil in diameter) is mounted in a lead bonder apparatus, and the wire is fed through a glass or tungsten carbide *capillary*. The capillary is brought down and the combination of force and temperature bonds the wires to the stripe contact. After raising the capillary again, an automatic spark flame jet is swept past the wire to remove the "tail" of the Au, as shown in Figure 3.7.

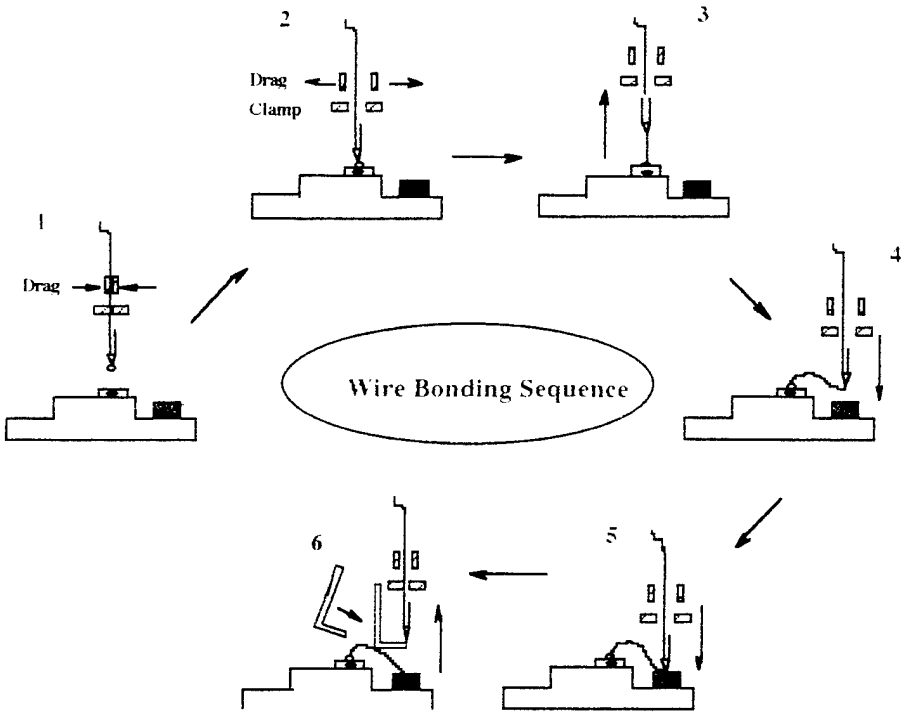

Figure 3.8. Wire Bonding Sequence for Laser Diodes.

Since InAs material is mechanically softer than GaAs material, several remodifications, such as force, power, time, and bonding temperature, had to be changed to avoid contact and epitaxial layer damage. This bonding damage is apparent when measuring the current-voltage characteristics.

The dials that set the bonding parameters are:

SEARCH	regulates the height of the Bonding Head in the Search position
FORCE	regulates downward force exerted by the Capillary on the bond
TIME	regulates duration of the ultrasonic energy and bonding force pulse
POWER	regulates the ultrasonic power level
LOOP	sets the height to which the capillary will rise after performing the first bond

4. Optimization of Technology and Future Trends

Up to now, the longwavelength lasers in the 3.2 μm region are broad-area diode lasers with emitting aperture of 100 μm. Typical power that are being emitted for these lasers are within 200 mW with total quantum efficiency of 15 - 18 %. The highest average peak power for a 100 μm aperture is 260 mW with a threshold current density of 40 A/cm^2 for long cavity length. The internal losses, α_i , for these double heterostructure are estimated in the range of 50 cm^{-1} - 100 cm^{-1}. The large losses is inhibited to the current leakages and other contributed factors which can not be explained at this time. In order to reduce the current leakage spreading from the broad-area, a dielectric passivation such as SiO_2 or Al_2O_3 are being investigated. Futhermore, by depositing SiO_2 or Al_2O_3 between the stripes, the diodes can be mounted p-down which will provide better current propagation along the stripe.

4.1. Dielectric Passivation on the InAsSbP/InAsSb/InAs Lasers

The method and procedure to produce passivation onto a laser structure to obtain current and optical confinement consists of a simple direct patterning by photolithography

techniques, and the deposition of a dielectric layer onto the semiconductor surface by electron-beam evpoartion. The procedure to deposit passivation to the lasers is outline below:

1) Create a 100 μm resist linewidth by photolithography

2) Etch at least 0.10 - 0.12 μm of the p-doped InAs cap layer

3) Remove photoresist by immersing into acetone

4) Apply new layer of photoresist to create a 50 μm stripe width directly on top of the 100 μm etch region.

5) Insert the patterned sample into the electron -beam chamber, and deposit a layer of Al_2O_3 (1.0 μm - 2.0 μm). Keep depostion rate within 4 Å/second with maximum power of 24 %.

6) Remove the samples and immerse them into an acetone bath for at least 1 minutes remove the remaining photoresist.

7) Finally, deposit a thick layer of metal film (TiPt/Au)over the entire area of the sample.

8) Anneal the p-contact layer at temperature of 300 - 320 °C for 3 - 4 minutes under forming gas.

9) Lap and polish n-side substrate to a thickness of 120 μm followed by another n-contact deposition of AuGe/Ni/Au.

10) Anneal n-contact layer at temperatures of 300 - 320 °C for 3 - 4 minutes.

5. Studies of Dielectric Coatings for Longwavlength Lasers

The design of a multilayer stack is a stack of alternating films of optical thicknesses, corresponding to one quarter ($\lambda/4$) of the design wavelength, but of two different refractive indices. These different refractive indices corresponds to a higher refractive index (H-

layer), and a lower refractive index (L-layer). A shorthand design of a multilayer stack can be interpreted as H-L-H-L-H-L-H-air, where the last layer is always a higher refractive index. To make these high reflective coatings suitable for laser devices, two requirements are necessary: thickness uniformity and thickness control. To ensure good thickness uniformity over the whole region of the substrate or mirrors, a proper position of the material sources and samples is necessary. To achieve the exact thickness of the evaporant material, which are required in AR/HR laser coating design, a thickness control has to be provided at all time or during consecutive runs. The desired thickness is reached when the crystal quartz inside the evaporator monitors the material that is evaporating as shown Figure 5.1.

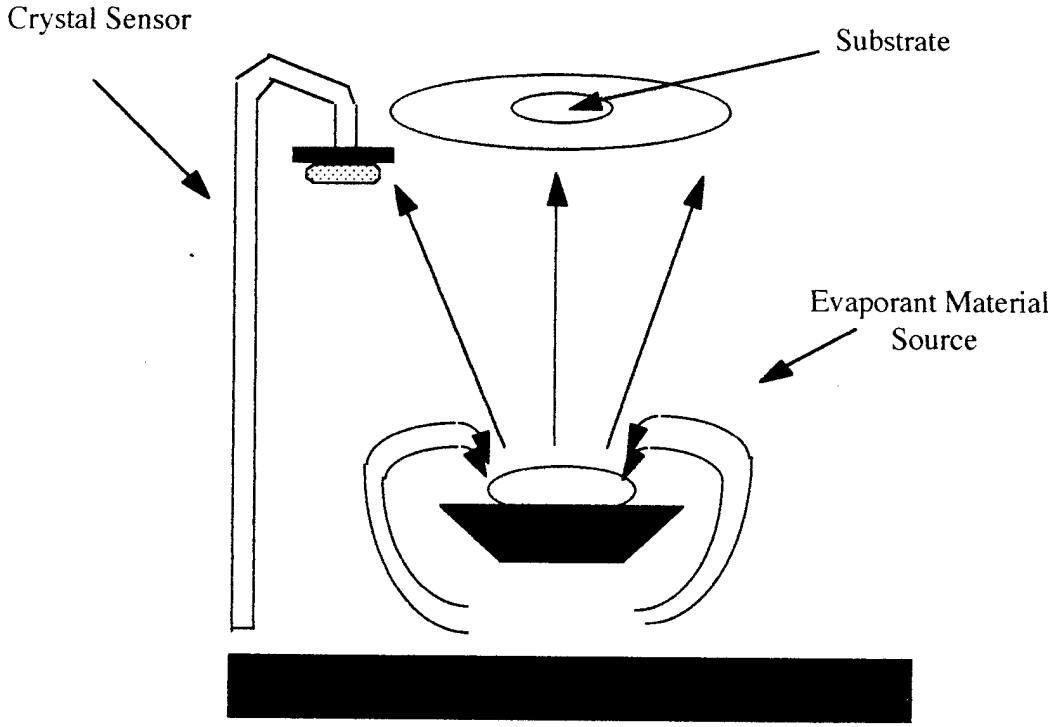

Figure 5.1. Schematic diagram of an evaporator depositing a material source.

The crystal quartz is caliberated by evaporating a source material, such as silicon or alumina oxide (Al_2O_3), to a thickness of 5000 Å. By utilizing Equation 5.1, the tooling factor can be calculated and programmed into the evaporator system.

Equation 5.1:

$$\text{Toolong } \% = \frac{\text{Substrate Thickness}}{\text{Displayed Thickness}} \text{ X } 100$$

This tooling calibration is necessary in mirror coating design if control thicknesses is required. If the tooling factor has not been corrected into the e-beam system, then a 10-20 % thickness error can be obtained. Such error can have a impact on coating design.

Following a system calibration, the refractive index of the material must be known to design a multilayer coating layers. The thickness and the reflection of the mirrors are dependent upon the refractive index of the source material as illustrated in Equation 5.2 and Equation 5.3. If the refractive index is not known or misused properly, then the desire reflectivity of a AR mirror coating can not be obtain. The refractive index of a material can be obtain by using a ellipsometer system. A spectroscopic elilipsometer is capable of dtermining the thickness of a film and film multilayers to accuracy's of a few angstroms. Furthermore, it has the ability to calculate the complex refractive index of materials over entire certain range. At the present time, the refractive index of Si (3.84) and Al_2O_3 (1.60) are obtain from text references.

Equation 5.2:

$$X_1(n_H) = \frac{\lambda}{4 * n_H}$$

Equation 5.3:

$$R = \left[\frac{1-\left(\left(\frac{n_H}{n_L}\right) * \frac{n_H^2}{n_s}\right)}{1+\left(\left(\frac{n_H}{n_L}\right) * \frac{n_H^2}{n_s}\right)} \right]$$

To study the reflectivity and method to design antireflection coating (ARCs) for longwavelength lasers, several coating experiments is carried out in which a two layer multilayer stack is condisered for the back mirrors. In the design of ARCs, several authors have used SiO_2/Si and using arsenic trisulphide and magnesium fluoride as the high and low refractive index layers. Where others have used Si and Al_2O_3 multilayer design. In the design of ARC's for 3.2 μm lasers, Si and Al_2O_3 are being study to improve the performance of these lasers such as low threshold current, high quantum efficiency, and perhaps a higher operating temperature.

Due to equipment limitation such as the use of a ellipsometer, the refractive index of Si and Al_2O_3 were take from references. The reflectance of a multilayer stack coating was measured by using a FTIR system to detect the transmittance between 2.5 μm to 30 μm wavelength. By depositing a multilayer stack of of Si (2270 Å) and Al_2O_3 (5469 Å), onto a quartz glass, a reflectance of 96 % is predicted according to equation 5.2 and 5.3. However, experiments shows that the reflectance is 97% for a 3.5 pairs multilayer stack as shown in Figure 5.2.

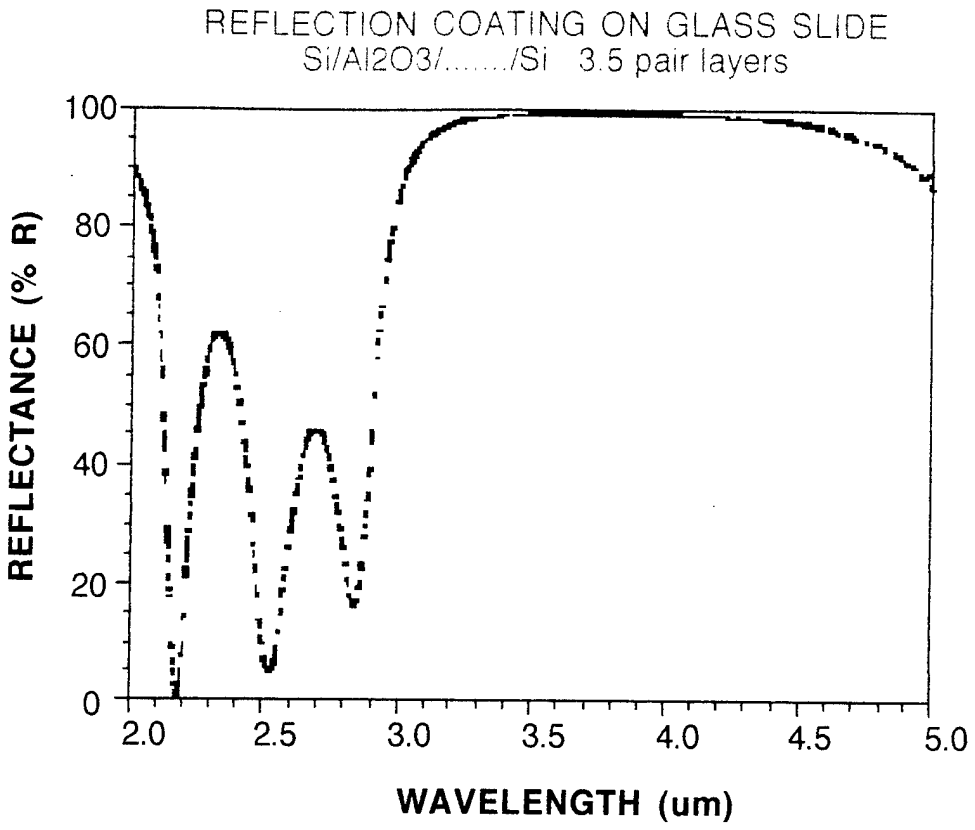

Figure 5.2. Reflectance spectra of a seven-layer antireflective coating (ARC) on an glass substrate for wavlength 3.5 μm range.

To study the wider applicabililty of the method to design ARC coating, a variety of layers is carried out in which differents pairs of layers is deposited to a glass substrate. A number of pairs layers are applied to evaluate the design reflectance for a wavlength of 3.5 μm. By evaporating 1.5 pairs of Si/Al_2O_3, the calculated reflectivity of the back mirror is 77.5 % . Experimentally, the sample substrate measured a reflectivity of 75 % as shown Figure 5.3, which is close to the calculated reflectance in Equation 5.3.

Two additional experiments were done to determine the transmittance variations for 2.5 and 3.5 pair layers. By evaporating 2.5 pair layers and 3.5 pair layers of Si/Al_2O_3 multilayer, the variation of additional layers in the stack increases the reflectance as shown in Figure 5.3.

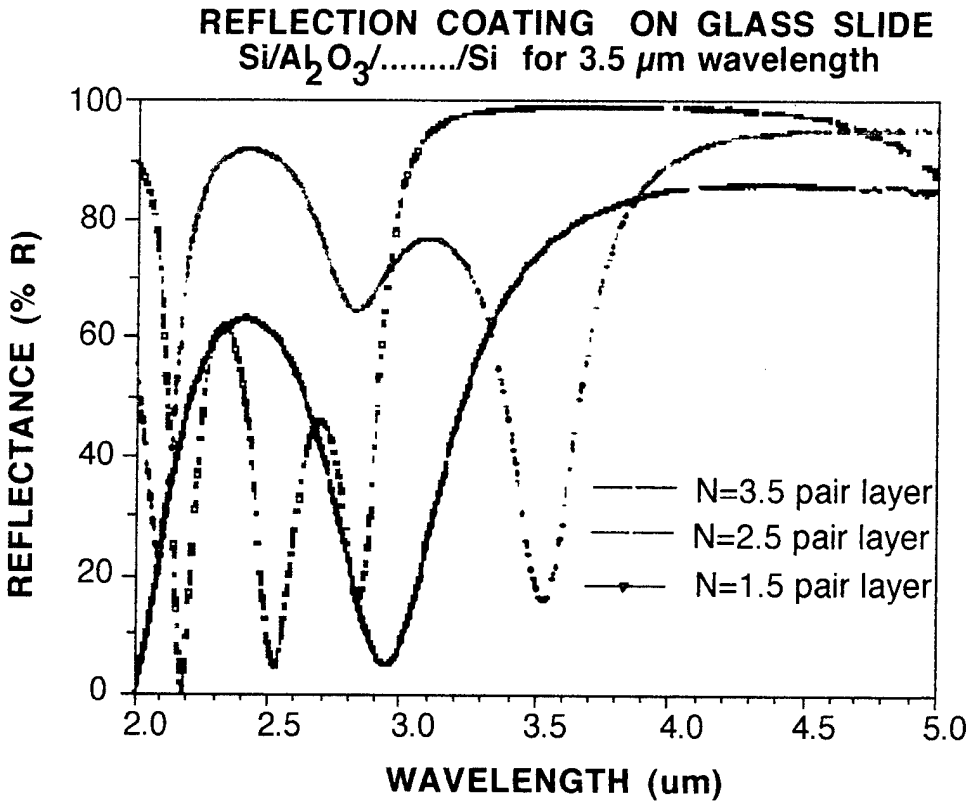

Figure 5.3. Comparison of the reflectance with N number of pair layers in a midinfrared region.

As shown in Figure 5.3, a 3.5 pair layers of Si/Al_2O_3 the measured reflectance is 97 % at 3.5 μm. According to Equation 5.3 the reflectivity is 96 %. In the case of the third experiment, the measured reflectance did not correspond to the calculated 89%. The difference among the three samples is that the last sample was left over night and with no cleaning of the chamber. Whereas, the first and second sample was evaporated consecutively and cleaned after each run. Therefore, in order to obtain good antireflecting coatings, it is necessary to clean the chamber after each run.

Future Work for Technology:

- Continue in optimizing the SiO_2
- Designing a new set mask for the longwavelength RW lasers.
- Develop new solution for the InAs and InAsSbP separately to avoid large undercut of the InAs layer.
- Optimize conditions of SiO2, Silicon and Al_2O_3 for antireflective coatings.

Chapter 4

Laser Characterization

Outline:

I. Introduction.

II. Experimental Results.

1. measurement set-up/ types of measurements.
2. improvement of internal loss.
3. improvement of threshold current density.
4. comparison of pulse and cw operation.
5. far-field light intensity distribution.
6. threshold current density vs stripe width.
7. peak wavelength vs temperature and cavity length.
8. typical spectra for 3 cavity lengths/ 2 stripe widths.
9. abnormal dependence of threshold current density on temperature in Multiple Quantum Well lasers.
10. preliminary results for DH lasers grown on GaSb.
11. summary of our best results.

III. Appendix: short summary of lasers characterized from April to Oct. 1996.

I. Introduction

Previous chapters dealt with material growth issues, wafer characterization, and wafer processing. The next step is laser characterization, followed by interpretation of the results, providing feedback to material growth and wafer processing.
Laser characterization also allows to evaluate their performance in prospective applications, e.g., laboratory spectroscopy of molecules in the mid-infrared, remote monitoring of gaseous pollutants, and chemical reaction control.

The specific problem of characterization of lasers in this infrared spectral region is considerable background radiation, and dark current of detectors. To minimize these undesirable features of light measurement in the infrared, the following techniques can be used: AC coupling of electrical signals, lock-in detection, or the active baseline subtraction with a boxcar. The choice depends on duty cycle of injection current, and type of measurement.

II. Experimental Results.

1. Measurement set-up/ types of measurements.

Fig.4.1 shows a schematic of the measurement set-up. All measurements are automated and controlled with a computer. Since we use short pulses, this set-up incorporates a boxcar averager. We can directly measure the light power vs current characteristics, the far-field light intensity distribution, spectra, and I-V characteristics. From these measurements we can determine threshold current densities, To, differential efficiencies, internal loss of the material, transparency current of a laser, wavelength shifts, and series resistance.

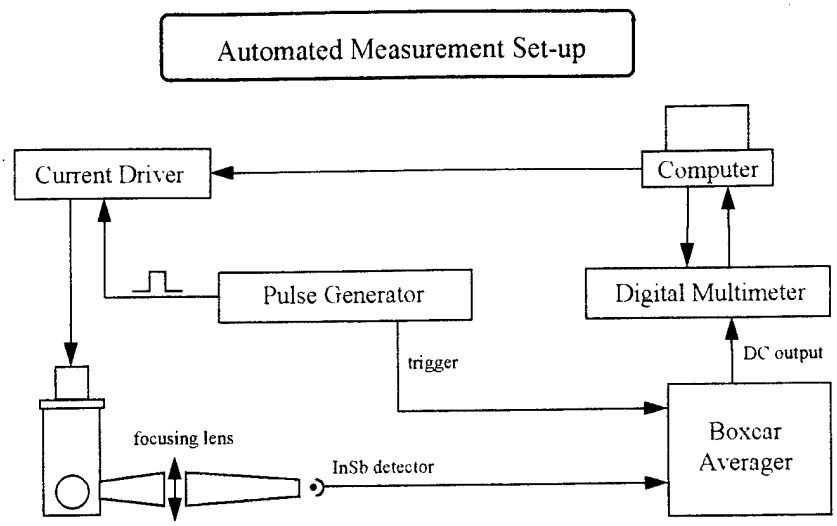

Can measure:
- light power vs current
- far field
- spectra
- I - V

Can determine:
- threshold current/density
- To
- efficiencies
- internal loss
- transparency current
- wavelength shifts
- series resistance

Fig.4.1. Automated measurement set-up

Laser diodes with cavity length varying from 300 mm to 1800 mm were prepared without mirror coating and light characteristics were recorded in pulse operation and in cw operations using the above setup system . In measuring the emitted power from a single diode, an InSb detector was used. The measurements of light power are based on a calibrated InSb detector. Its responsivity, % peak response for a given wavelength, and trans-impedance gain of a pre-amplifier are given by the manufacture (EG&G Judson), and yield a correspondence between impingent light power and output voltage. This voltage is measured with a calibrated boxcar averager, additionally controlled with an oscilloscope. To avoid saturation of the detector, we use neutral density filters; linearity of the light power is also assured by a matched pre-amplifier, which saturates when the input exceeds a linear regime level. The filters were carefully positioned to avoid

due to reflections at optical (sapphire) components' surfaces were taken into account using transmittance of windows given by particular manufacturers. Finally, the light power is multiplied by two assuming equal emission from two facets.

Fig.4.2 illustrates the basic measurement of light power vs current characteristics. From measurements we can determine several basic key parameters such as threshold current densities J_{th}, and differential quantum efficiencies η_d. Measurements for several temperatures yield the characteristic temperature T_o. Dependencies of J_{th} and differential efficiency at various cavity lengths allows us to estimate the internal loss and the transparency current J_o of a laser structure.

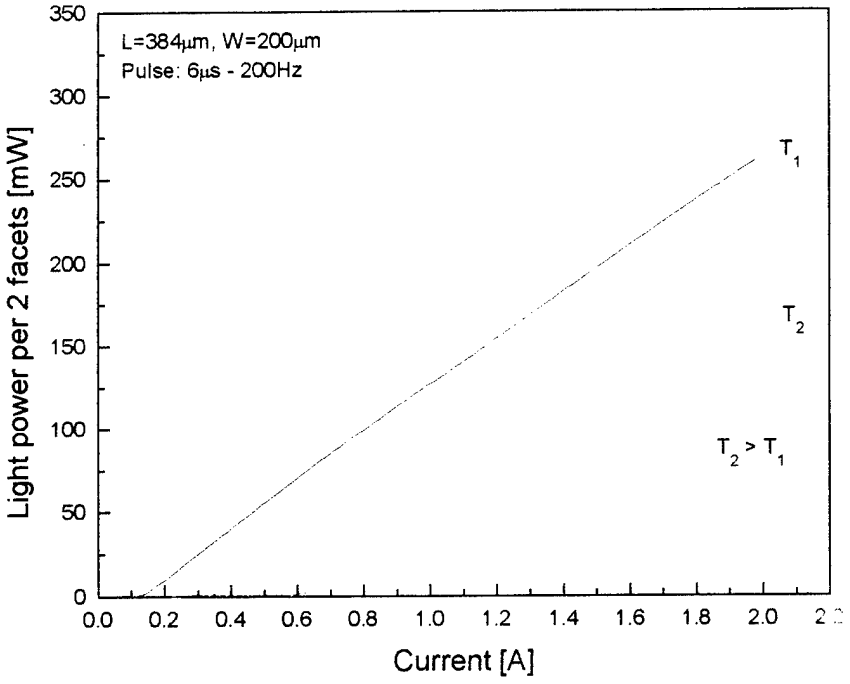

Fig.4.2. Light-current characteristics of an InAsSb/InAsSbP/InAs diode laser

2. Improvement of internal loss.

Since the start of this contract, growth conditions and fabrication of the lasers have been optimized. Fig.4.3 shows our progress in the quality of material: the internal loss, as determined from the plot of inverse differential efficiency vs. cavity length, has been reduced from about 100 cm^{-1} to 3.3 cm^{-1}, which is the lowest value reported in literature.

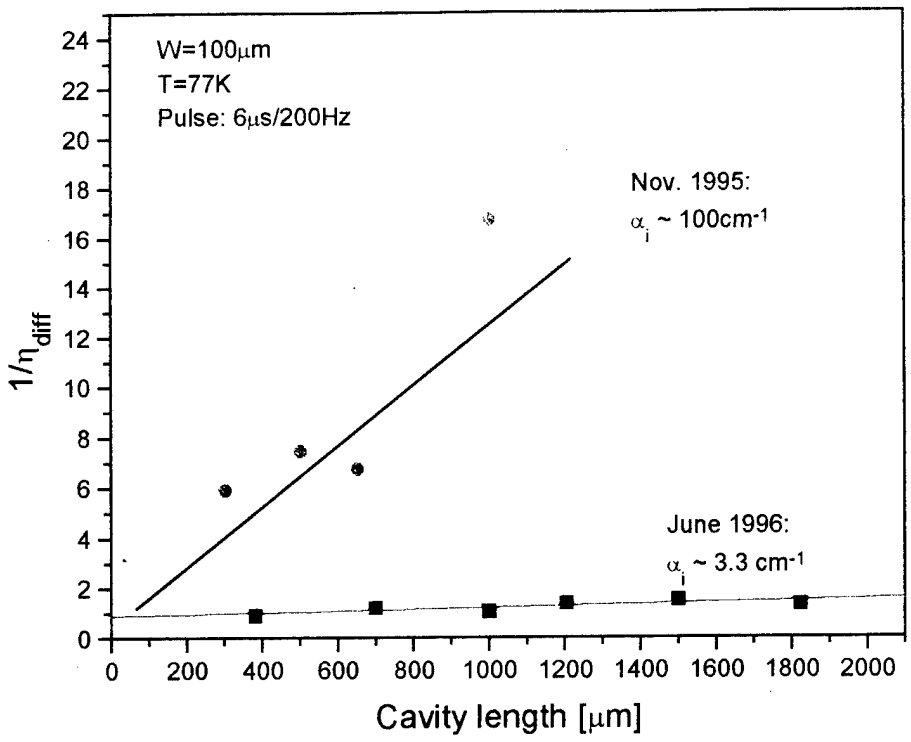

Fig.4.3. Inverse differential efficiency vs cavity length.

To characterize the basic material properties of the epitaxial structure, the differential quantum efficiency is measured as a function of cavity length for the 100 μm broad-area laser. Fig. 4.3 shows the reciprocal of measured total differential quantum efficiency, i.e., both facets, as a function of bar length. The linear approximation based upon the equation of the efficiency of a laser diode consists of the following equation:

$$\eta_{ext}^{-1} = \eta_{int}^{-1}\left(\frac{\alpha L}{\ln(1/R)} + 1\right)$$

yields a distributed loss coefficient of 3.3 cm^{-1}. The value of the distributed loss is the lowest internal loss reported comparable to other DH Sb-based lasers.

3. Improvement of threshold current density.

The internal transparency current is determined by measuring the threshold current density as a function of diode cavity length as shown in Fig. 4.4. The J_{th} vs 1/L of DH InAsSbP/InAsSb/InAs diode lasers (Fig.4.4) shows that threshold current densities have been reduced more than 10 times, yielding the transparency current of about 34A/cm^2, which is the best value reported in literature. In both Fig.4.3 and 4.4 we can also see that the scattering of measurement points is greatly reduced in recent series, which indicates that both processing and measurements give reliable results.

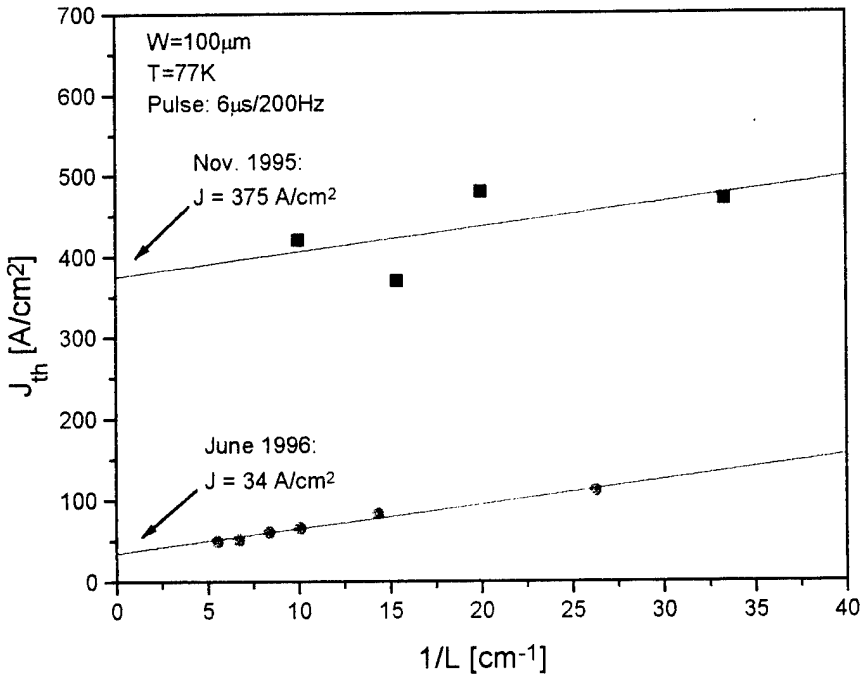

Fig.4.4. Threshold current density vs inverse cavity length of double heterostructure InAsSbP/InAsSb/InAs at 77K

4. Comparison of pulse and cw operation.

Shown in Fig.4.5 (a) is a comparison of pulsed and cw operation. Whereas in pulse-mode the light-current characteristics do not exhibit any saturation, it is not a case in continuous operation. This difference comes from the fact that the average heat to be dissipated is about 1000 times higher in cw, since the duty cycle of pulses used is $\sim 10^{-3}$. It can be noted that up to about 105K the differential efficiency is practically the same in both modes of operation; furthermore, all these characteristics are reversible (i.e., there is no damage to the laser). The rapid decrease of emitted light power above the critical temperature/current may indicate an existence of a positive feedback between absorption of light and the increase of laser's temperature; these effects can be utilized in a study of thermal properties of the material and bonding.

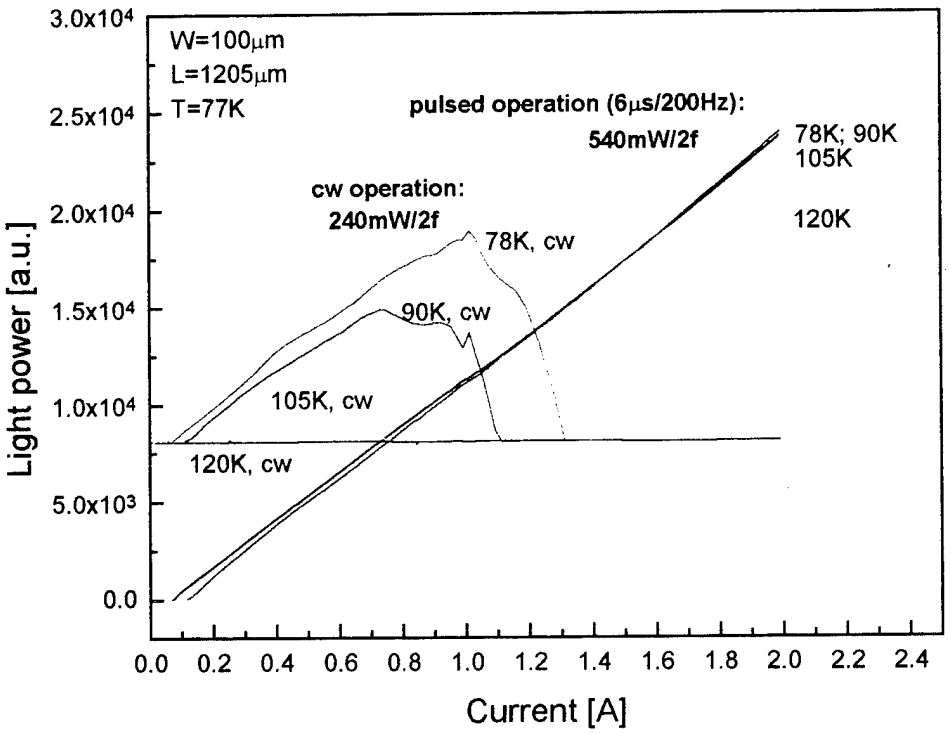

Fig.4.5 (a) Light-current characteristics of DH InAsSbP/InAsSb/InAs diode laser operating under pulse and continuous wave operation at various temperatures from 77 K up to 120K.

It is notable that the emitted light power - as shown in Fig.4.5 (a) can reach almost 50% of that in pulse operation at 77K. The demonstrated operation at 300mW cw is the highest value reported in literature. Several DH InAsSbP/InAsSb/InAs lasers were measured for high power in pulse operation at low temperature 77K. Fig. 4.5 (b) is an example of a double heterostructure laser with 100 μm aperture (wafer #99) capable of emitting an output power of 660 mW per 2 facets at 77K. The differential quantum efficiency of most lasers are typically over 80 %. The inset of Fig. 4.5 (b) is the same diode laser operating at a highest temperature of 220K at a operating current of more than 15 A.

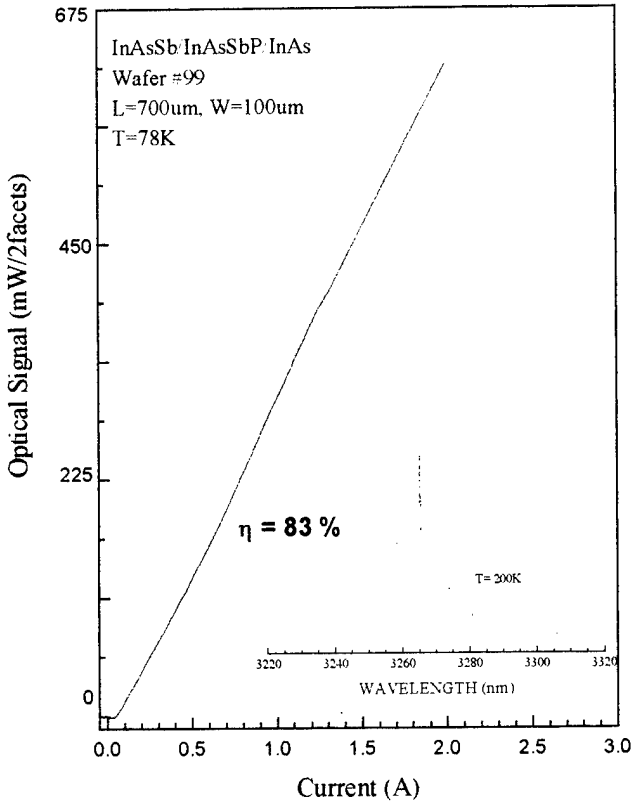

Fig. 4.5. (b) Light - current characteristics of a double heterostructure diode laser (wafer #99) with cavity length 700 μm and stripe width of 100 μm operating under pulse operation at 77K.

In the case of multiple quantum well lasers (superlattice structures), the high output power that has been obtain from 100 μm aperture is 900 mW per two facets under pulse operation (6us - 200 Hz) at 90K. To reach this power was possible by injecting currents of 5 A as shown in Fig. 4.6. In studying the characteristics of such MQW structures over DH lasers, the temperature dependence of threshold current density J_{th} of MQW is compared to that of DH laser for cavity lengths from 700 μm up to 1200 μm. Measurements showed that J_{th} of MQW laser have at least 2 times lower J_{th} for the entire temperature range of 90 K up to 140K. It is to believe that the low J_{th} is mainly due to the effect of compressive strain on the band structure and consequently on optical properties such as gain and radiative recombination current. To confirm this argument, theoretical calculation have been done. Such calculations and interpretation are explained deeply in Chapter 5.

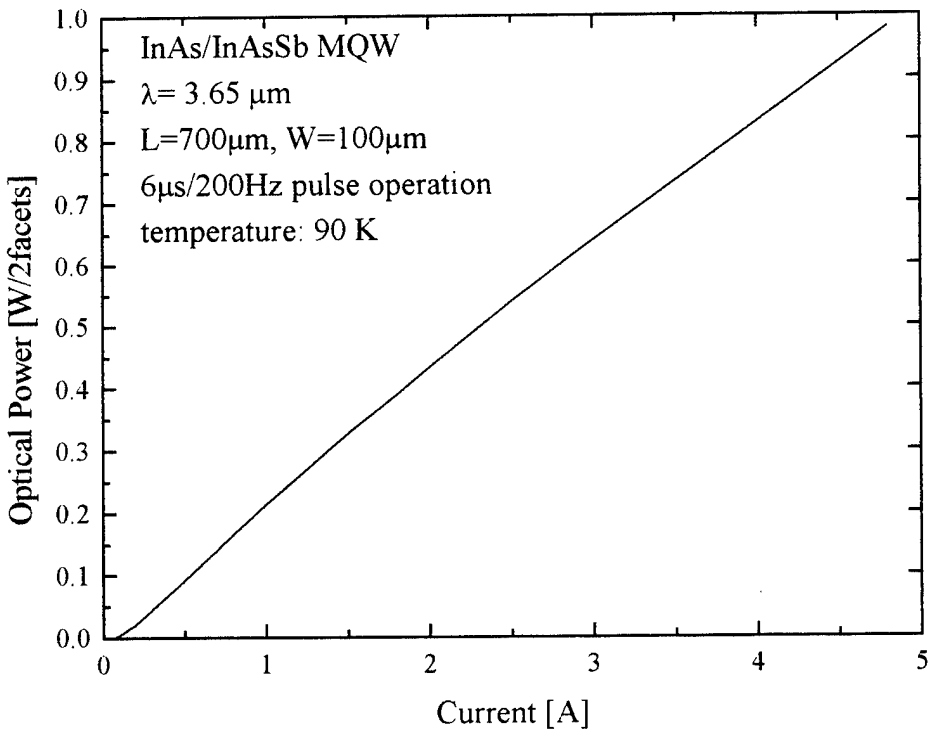

Fig.4.6. Light-current characteristics of a MQW InAsSb/InAsSbP/InAs at 90K.

5. Far-field light intensity distribution.

Fig.4.7 shows a smooth far-field light distribution. The FWHM value of 34^0 in the direction perpendicular to the junction is the best value reported for this material system. In general, the measured and calculated values of far-field in the perpendicular direction are in a good agreement, as discussed in Chapter 5.

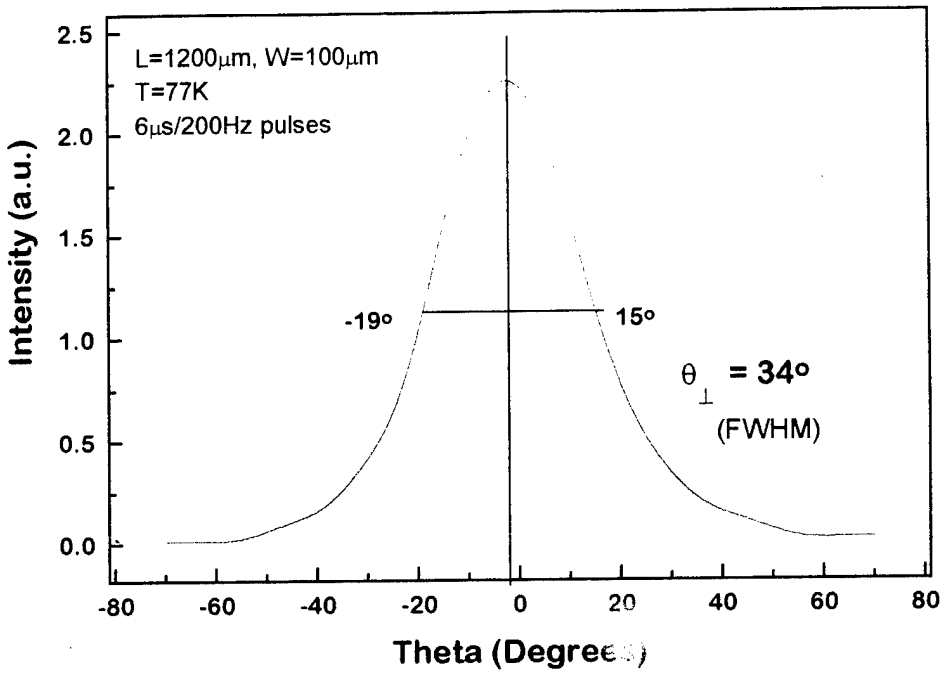

Fig.4.7. Far-field light intensity distribution.

Further studies are being made to the measurements of far-field in the perpendicular and parallel direction. Such studies consists of temperature and cavity length dependencies with respect to DH and SCH lasers.

6. Threshold current vs stripe width.

Another dependence of interest is that of threshold current density vs stripe width (Fig.4.8).

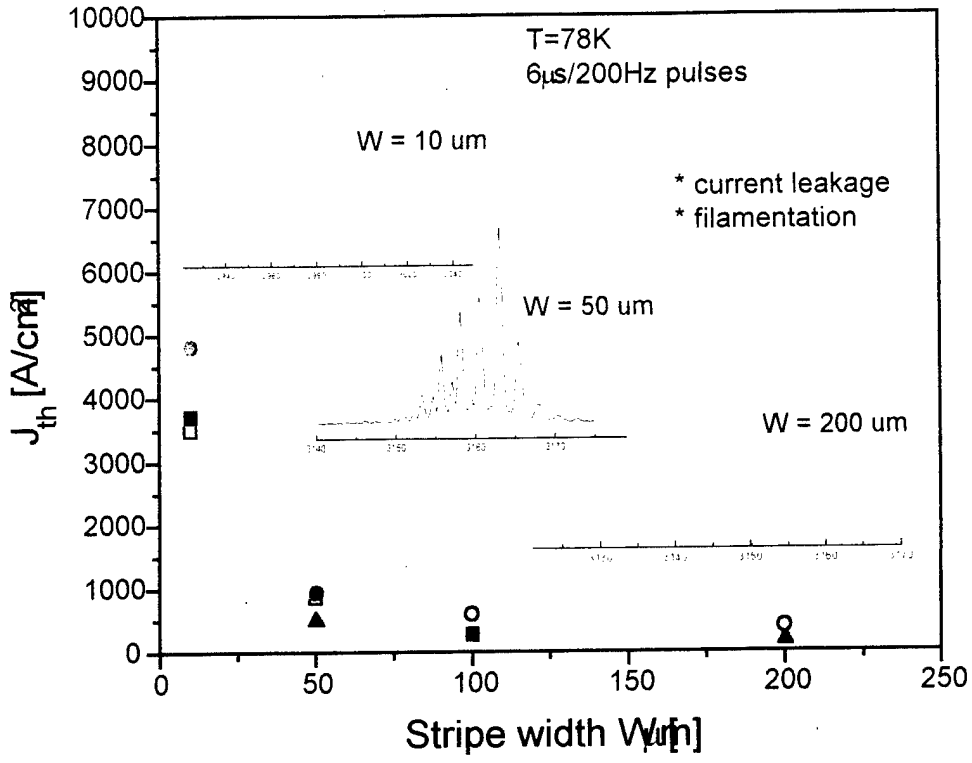

Fig.4.8. Threshold current density vs stripe width of double heterostructure InAsSbP/InAsSb/InAs laser structure under pulse operation at 77K.

As can be seen, we need to use relatively broad-stripe lasers (~100μm to 200μm) to obtain lowest values of threshold current densities. It is because of the lateral current leakage: part of current lost due to the lateral spreading is higher in narrow-stripe lasers, possibly even approaching 90% of the injected current as can be estimated from Fig.4.8. However, light spectra are more regular in narrow-stripe lasers, which can be understood as a result of reduced filamentation.

7. Peak wavelength vs temperature and cavity length.

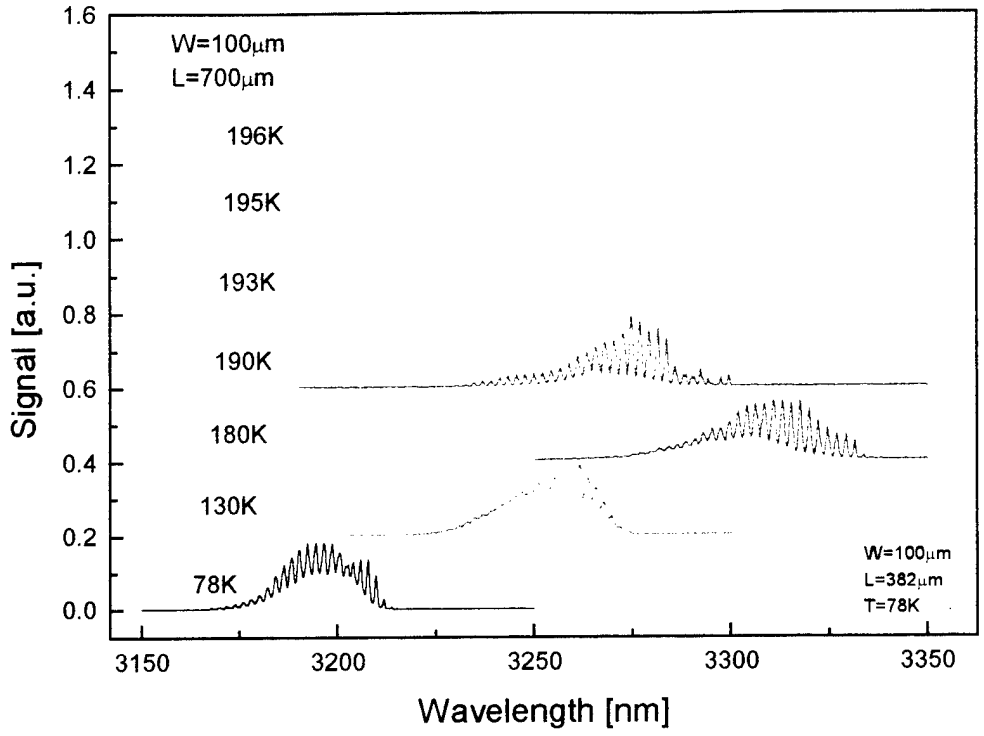

Fig.4.9. Wavelength tuning with temperature for DH InAsSbP/InAsSb/InAs diode lasers.

Fig.4.9 shows how wavelength depends on temperature. Up to ~180K, it shifts towards longer waves, which is primarily due to the decrease of energy gap with temperature. At higher temperatures, the wavelength starts to shift toward shorter waves which may by explained as follows: with increasing temperature, the density of thermally generated electron-hole pairs in the originally p- and n-doped cladding layers becomes comparable to the density of extrinsic carriers (in other words, the region of temperatures changes from extrinsic to intrinsic in this material; difference between p- and n-doping gradually vanishes). As a result, the density of injected excess carriers to the active region decreases for a given current, so that reaching a threshold current or a given light power requires higher injection current. As long as temperature is in the extrinsic region, this leads to a usual increase of threshold current density; however, after exceeding a

characteristic temperature of transition between the extrinsic and intrinsic regions, the increase of threshold current becomes rapid. Additionally, it may be further increased by a positive feedback from the high current to the increase of temperature, possibly also including optical absorption, as discussed in comments to Fig.4.5. Finally, the rapidly increased current leads to an increase of separation between quasi-Fermi levels for electrons and holes, yielding shorter lasing wavelengths.

Another feature of spectra shown in Fig.4.9 is a more regular Fabry-Perot mode structure at higher temperatures. It can be understood as reduced effects of filamentation due to smaller lasing portion of the active region at high temperatures.

Fig.4.10 shows a typical dependence of wavelength on cavity length. The increase of wavelength can be utilized to tune the lasers within about 40nm. This dependence can be explained as a decrease of the quasi-Fermi levels separation due to the reduced threshold current densities (lower mirror loss) in longer cavity lasers.

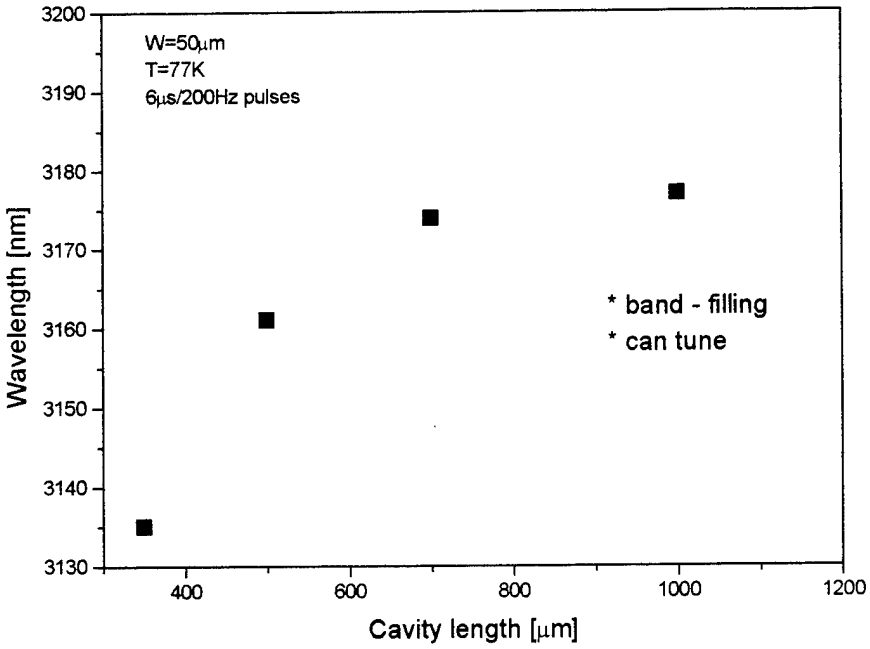

Fig.4.10. Peak wavelength vs cavity length.

8. Typical spectra for 3 cavity lengths/ 2 stripe widths.

Fig.4.11 shows how spectra change with cavity length. The vanishing of the Fabry-Perot mode structure can be attributed to filamentation combined with material nonuniformity. The existence of filamentation is evident in many spectra, e.g., in the bottom one of Fig.4.11, showing more than 1 set of longitudinal modes. The reasons of the qualitative change of spectra with increasing cavity length are the smaller separation of longitudinal modes, and their broadening. The former one is an elementary property of an optical resonator, while the latter one is most probably due to effects of nonuniformity of the refractive index in the cavity, more pronounced in longer/wider cavities and/or higher currents (the opposite effect of temperature shown in Fig.4.9 seems to support this explanation). One more effect can be suspected to come into play in high-loss material: it is the damping of optical cavity oscillations if the internal loss becomes comparable to 1/L, which leads to significant broadening of the Fabry-Perot modes. Some wafers showed such high internal loss, but systematic study allowing to extract this effect has not been done yet.

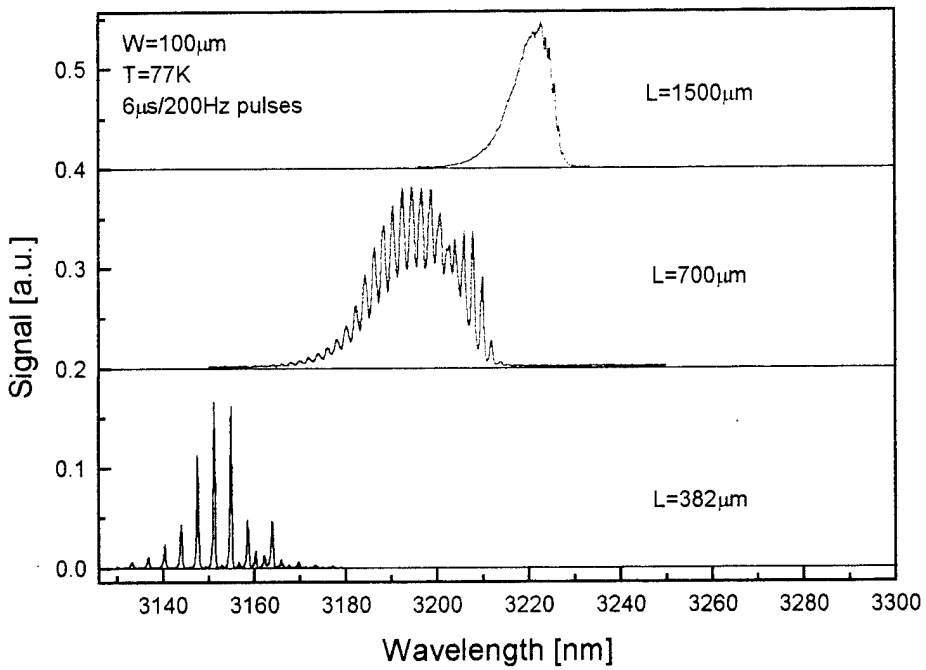

Fig.4.11. Spectral distribution of light power for 3 cavity lengths (100μm).

Shown in Fig.4.12 are the same effects, but in broader stripe lasers (200μm instead of previous 100μm). On top of the discussed effects, we can see an irregular envelope of the bottom spectrum which is a result of non-uniformity of energy gap of the material, whereas the higher base of spectra in long-cavity lasers can be explained - as previously - as a result of nonuniformity of the refractive index of the material; both are more pronounced in wider-stripe lasers.

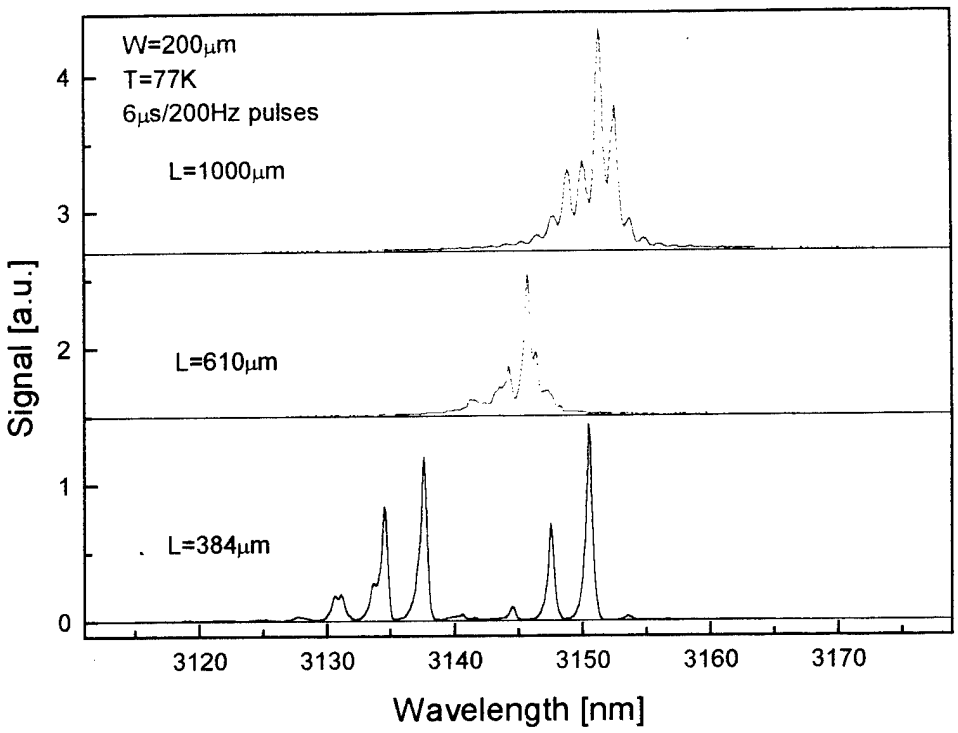

Fig.4.12. Spectral distribution of light power for 3 cavity lengths (W=200μm).

9. Abnormal dependence of threshold current density on temperature in Multiple Quantum Well lasers.

All nine measured MQW lasers exhibited a non-exponential increase of the threshold current on temperature. In six of them, threshold current was minimum between

80K and 90K; in the remaining 3 lasers, it seemed to have a minimum below 78K. Above these temperatures, the increase of threshold current follows a usual exponential dependence, characterized by one parameter - the To; Fig.4.13 depicts a typical example in these lasers.

Based on measurements of 9 lasers, we have not found a correlation between the occurrence of this abnormality and cavity length, lower/higher threshold current, or quality of indium used for die bonding. This abnormality seems to be a property of the structure/material; we have suggested an incomplete thermalization of carriers in the wells below ~80 to 90K to explain it. In any case, this effect yields about 2 times lower threshold current in MQW lasers compared to corresponding DH ones in the temperature range between 90 and 140K.

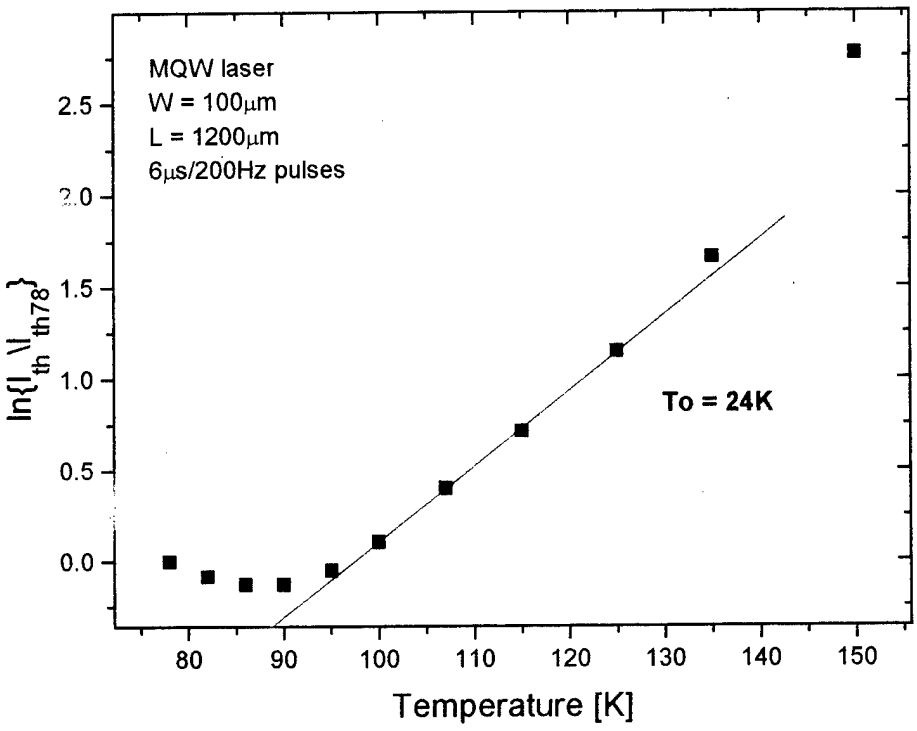

Fig.4.13. Abnormal dependence of threshold current on temperature in MQW lasers.

operating temperature is the T_o, which attributes to many mechanisms within the structure and bonding technology as well.

10. Preliminary results for DH lasers grown on GaSb.

We have recently grown 3 wafers on GaSb substrate to obtain longer wavelengths. So far, the lowest threshold current is 0.5A, the lowest threshold current density 1kA/cm^2, and the highest light power 30mW. The wavelength is 3.6μm. Apart from the high thresholds, the series resistance of these lasers is greater than 2 Ohm. Furthermore, we have found this new material to be more difficult to cleave. However, we have only grown, processed, and measured one batch of these lasers, such that these results should only be considered as preliminary.

11. Summary of our best results.

* P_{max} = 660mW/2 facets in pulse operation
  P_{max} = 0.9W/2f in pulse operation (MQW)
  P_{max} = 0.3W/2f in cw
* η_{diff} = 90%
* α_i = 3.3cm^{-1}
* J_{th} = 40A/cm^2
* To = 42K
* Rs = 0.2 Ω

III. Appendix. Short summary of lasers characterized from April to October 1996

Agency: DARPA/U.S Army # DAA04--95-1-0343
Laser Structure: DH InAsSb/InAsSbP/InAs
Efierel Reactor

W=100 μm

Wafer#	L(μm)	Jth (A/cm^2)	To (K)	P(mW/2facets)	λ (nm)
806	470	638	24	30mW	3082
809	700	283	24	20mW	3102
813	540	148	42	24mW	3121
817	500	130	23	35mW	3182
817	800	105	26	28mW	3193
817	1000	95	28	25mW	3195
818	488	102	20	30mW	3152
833-sch	470	851	----	6mW	-----
834-sch	482	290	22	10mW	2930
837	-----	------	-----	-----	-----
841	482	124	----	40mW	-----
843	500	88	31	47mW	3150
843	823	48.6	32	250mW:pulse 56mW:CW	3165
843	1000	40	35	90mW	3180
847	300	516	20	2.5mW	3078
847	500	321	23	4.62mW	3080
847	1000	178	25	6.2mW	3098
851	500	184	21	15mW	3085
851	823	134	23	12mW	-----
851	1000	125	23	12mW	-----
854	488	152	20	15mW	3085
854	800	107	22	12mW	----
854	1000	100	23	12mW	----
879	382	340	18	11mW	3060
879	700	212	21	22mW	3095
879	1000	170	21	24mW	3110
883	282	265	20	260mW	3081
883	382	202	20	120mw	3085
883	700	114	23	227mw	3090
883	1000	90	23	120mW	3105
1003	400	----	-----	-----	-----
1051	400	500	30	126mW	3178
1051	500	480	29	140mW	3202
1051	1000	300	34	135mW	3212
1051	1200	266	35	130mW	3225
1071	382	524	19	20mW	3126
1082	360	305	18	146mW	3187
1082	676	355	20	115mW	3216

1082	1000	230	21	110mW	3215
1085	382	157	22	180mW	3184
1085	676	178	23	115mW	3186
1085	1000	150	25	110mW	3190
1098	382	-----	-----	-----	-----
1099	382	1.520K	-----	56mW	-------
122	382	84	25	365	3195

InAsSb/InAsSbP/GaSb

1179	400	1700	-----	10 mW	-----
1179	700	1700	------	3 mW	3640
1185	700	1300	-----	3 mW	3670
1187	400	1200	------	30 mW	3590
1187	700	1000	-----	10 mW	3640

W=200 μm, 50 μm Efierel Reactor

	W(μm)	L(μm)				
818II	200μm	384	163	20	260mW	3136
818II	200μm	610	148	21	165mW	3146
818II	200μm	1000	120	22	138mW	3152
818III	50μm	300	470	20	173mW	3187
818III	50μm	500	480	21	80mW	3162
818III	50μm	650	370	21	82mW	3195
818III	50μm	1000	420	22	27mW	3193

EMCORE Reactor
Subject: 3-5μm InAsSb/InAsSbP/InAs

Wafer #	L(μm)	Jth (A/cm^2)	To (K)	P(mW/2facets)	λ (nm)
26	400	------	------	------	------
27	400	------	------	------	------
40	350	860	----	67mW	3135
40	500	880	19	65mW	3161
40	700	886	19	51mW	3174
40	1000	1800	16	9mW	3177
43	323	930	19	65mW	3030
43	500	700	17	67mW	3058
43	1000	660	17	15mW	3082
92	382	125	26	394mW	3164
92	700	84	26	470mW	3188
92	1029	58	----	560mW	3204
94	382	157	42	270mW	2998
94	382	159	40	200mW	3000

99	382	109	25	563mW	3152
99	700	65	28	660mW:pulse 300mW:CW	3190
99	1000	60	30	610mW	3206
99	1200	56	30	530mW	3215
99	1500	46	29	440mW	3222
99	1800	42	27	540mW	3230
109	382	105	23	630	3230
135-MQW	382	175	------	388	3565
135-MQW	700	107	------	900 @5A	3610

Chapter 5. Analysis and Modeling of the InAsSb/InPAsSb Double Heterostructure and Multiple Quantum Well lasers

5.1. Effect of inhomogeniety of material composion in active layers

The midwave infrared lasers for 3-5 μm are a very attractive source for several spectroscopi applications including atmostpheric trace gas analysis and medical diagnostics, because in this spectral region many atmostpheric species have strong rotational vibrational, and overtone absroption bands. As the signal-to-noise ratio in spectrosocopy is proportional to the square root of the laser power on the detector, the cw output power should be as high as possible. In the previous chapters, we reported high contiunous wave optical output power of 260 mW from an InAsSb diode lasers with emitting wavleneth at 3.2 μm at 78 K. The threshold current density as low as 48 A/cm2 with a characteristic temperature 30 K, differential efficiency higher than 80 % and a very low optical loss of 3.3 cm^{-1} are obtained. The high performance characteristics of the lasers are attributed to the improved material quality, especially, of InPAsSb cladding layers. In this section, the effect of inhomogeneous compositions of the active region on the laser characteristics are theoretically modeled and compared with experiment.

Figure 1 show the pulse and cw power versus curret curves at 78 K. High performances at power up to 650 mW in pulse operation and 240 mW at continuous wave operation are achieved without noticeable degradatation of the differential efficiency of 83 %. The higher power for pulse mode operation was only limited by current of our power source. The laser operated up to 200 K. The emitting spectrum at 200 K is shown in inset of Fig. 1. The Figure 2 shows the dependence of differential efficiency on cavity length, indicating that internal loss of the lasers is as low as 3.3 cm^{-1}. To our best knowledge, the cw power and

the differential efficiency are the highest values, while the optical loss is the lowest values, reported at this wavelength range from InAs- or GaSb-based materials.

We have compared the theoretical and experimental results of the dependence of J_{th} on the inverse cavity length (Fig. 4). In this calculation we only considered radiative recombination current. The Auger recombination and leakage current are negligible in this temperature range as determined by a recent photoluminescence experimet. The dotted line represent the calculation when assuming that the InAsSb can be represented by a uniform single-phase composition. The results show that the experimental data has a much stronger cavity length dependence than the recombination model predicts. This led us to consider the effect of the inhomogeneity of InAsSb active layer alloys. In our model, we assume that alloy has several phases such as ordered and disorderd strucutres with different compositions. The inhomogeneity of the composition in InAsSb and InPSb has been studied in a number of recent TEM experiments and the model parameters were obtained based on these experimental results. The solid lines in Fig. 4 represent the result of our new model, showing excellent agreement with experiment. These results indicate that the inhomogeneity of the materials may be the governing factor that inhibits laser performances at high temperature.

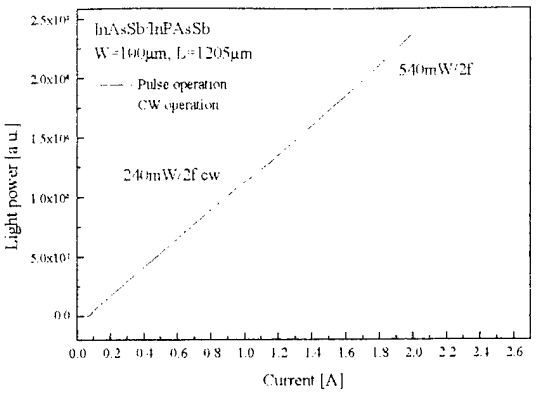

Fig. 1 The pulse and cw power versus curret curves at 78 K

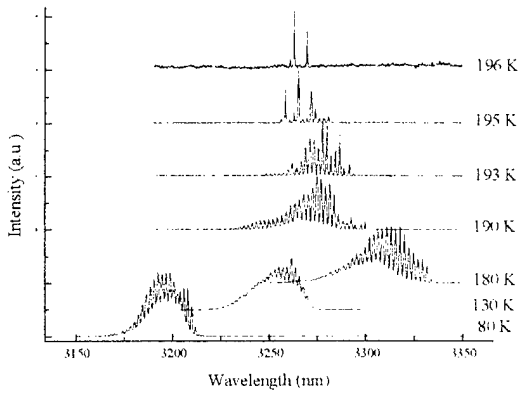

Fig. 2 Emission spectra for temperature range of 80 K to 196 K

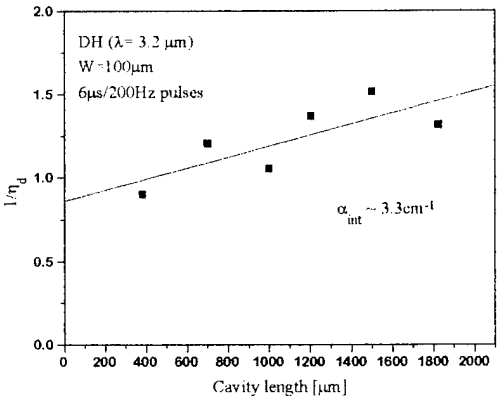

Fig. 3 Cavity length dependence of the differential efficiency

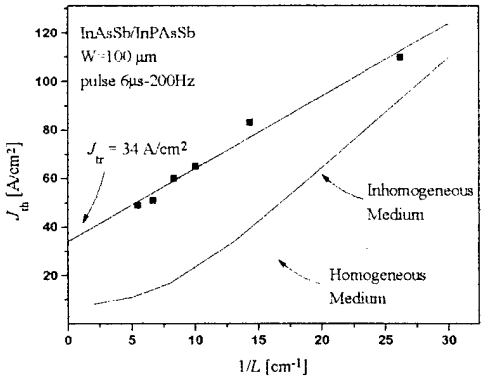

Fig. 4 Cavity length dependence of J_{th} The dotts and solid lines denote experiment and theory, respectively

5.2. Comparison of the Double Heterostructure and Multiple Quantum Well lasers

A number of groups have been developing antimony (Sb)-based materials for laser fabrication for this wavelength band. However, so far these lasers have suffered from a prohibitively strong increase of threshold current density, J_{th}, and decrease of differential efficieny, η_d, with an increase of temperature (i.e., low T_o). Characteristic temperature, T_o, of 20 ~ 40 K is typically measured for this wavelength range [1 ,2 ,3 ,4].

It has been argued that compressively strained multiple quantum well (MQW) structures would provide much better device performance than bulk double heterostructures (DH) for λ= 3 to 4 μm [1,2]. These efforts were based on theoretical predictions [5] that compressive strain combined with quantum-size effect would lower the in-plane effective mass of heavy-holes, reducing the threshold carrier density. A slight increase in T_o and improvement in the temperature dependence of differential efficiency in MQW lasers were reported [2].

Previously, we have reported a high power operation of an InAsSb/InPAsSb double heterostructure (DH) laser of up to 660 mW in pulse and 300 mW in cw mode with differential efficiency over 80 % [6]. To our best knowledge, the differential efficiency and output powers reported in that work were the highest among laser diodes for λ= 3 to 4 μm. The high performance of the devices was attributed to successful growth of high quality InAsSb and InPAsSb [6]. The purpose of this section is to show that the use of compressively strained quantum-well structure further enhances the device performance. For temperature range of 90 to 140 K, about 2 times lower J_{th} was obtained from QW lasers compared to bulk DH lasers grown on the same condition. The rate of increase in J_{th} with an increase in operating temperature is reduced by a factor of 3 below 120 K, with peak output power up to 1 W from two facets and a maximum operating temperature of 220 K.

MQW lasers were grown in an EMCORE vertical metalorganic chemical vapor deposition (MOCVD) reactor at a pressure of 60 Torr and a temperature of 490 °C, using trimethylindium (TMIn), trimethylantimony (TMSb), arsine (AsH_3) and phosphine (PH_3) for the group III and V sources, diethylzinc (DEZn) and tetraethyltin (TESn) for *n*- and *p*-dopants, respectively. The active region consists of 10 compressively strained quantum wells of $InAs_xSb_{1-x}$ embedded in a 1 μm-thick InAs layer which is surrounded by 1.2 μm-thick *n*- and *p*-$InAs_xSb_yP_{1-x-y}$ cladding layers. All layers except for the compressively strained $InAs_xSb_{1-x}$ layers are lattice-matched to the n^+-InAs substrate. Energy gaps of $InAs_xSb_{1-x}$ and $InAs_xSb_yP_{1-x-y}$ were estimated from photoluminescence to be 0.33 and 0.51 eV at room temperature, respectively. Each quantum well was nominally 100 Å thick and separated by 500 Å InAs barrier layers. A (004) x-ray rocking curve for the laser structure is shown in Fig. 1 with the schematic diagram of the MQW structure in the inset. The high crystalline quality of the active region is confirmed by the x-ray study where seventh orders of satellites can be seen. Similar DH lasers have been grown on the same growth condition with the following modifications: the MQW active region is replaced by a 1 μm-thick $InAs_xSb_{1-x}$ active layer with an energy gap of 0.38 eV, and the composition of $InAs_xSb_yP_{1-x-y}$ cladding layer was modified so that it is lattice-matched to the $InAs_xSb_{1-x}$ active layer. The latter change slightly lowers the energy gap of the cladding layers ($E_g \approx 0.50$ eV). The x-ray rocking-curve shows that relaxed lattice-mismatch of InAsSb is about 0.4 %, indicating Sb composition to be 6 % according to Vegard's law. Uncoated broad-area lasers of 100 μm width and cavity lengths from 300 to 1200 μm were fabricated for the measurements.

Figure 2 shows the optical output vs. injection current curves (*P-I* curves) of a MQW laser with a cavity length of 1200 μm measured at a wide range of temperatures (78 to 155 K). It is shown that while the threshold current increases with an increase in temperature above 90 K, the differential efficiency (the slopes of the *P-I* curves) appears to remain constant for the entire temperature range investigated. The differential efficiency was measured to be over 65 % up to 155 K. Such high values of differential

efficiency for the wide range of temperatures up to 155 K, to our best knowledge, have not been obtained for lasers based on conventional inter-band transition for $\lambda > 3.5$ μm [7]. The laser exhibited in pulse mode operation output power up to 1 W (power from two facets) (Fig. 3) where the device showed rapid failure. Examination on the failed device by microscope revealed damages in metal contact regions (burn) presumably due to heating by the high current injection, indicating that metallization and bonding technology are of primary importance in high power operation, rather than mirror damages. The cw and pulse output powers exceed the results of much more sophisticated lasers based on inter-subband transition [8], suggesting that conventional laser diodes based on inter-band transition may be preferred for high power performance. The lasers were bonded *p*-side up because of lack of available current confining technologies for low energy gap materials. Current confinement by deposition of SiO_2 layers is expected to enable *p*-side down bonding and consequently high-power and/or high-temperature operation.

The temperature dependence of threshold current density J_{th} of MQW is compared with that of DH lasers for cavity lengths of 700 μm and 1200 μm in Fig. 4 (a) and (b), respectively. Both figures show consistently that J_{th} of MQW lasers have ~ 2 times lower J_{th} for the entire temperature range investigated except for around 80 K. As discussed below, the lower J_{th} is mainly due to the effect of compressive strain on the band structure and consequently on optical properties such as gain and radiative recombination current. In order to directly confirm the argument that the compressive strain of quantum wells decreases J_{th}, as observed in our measurements, we performed a model calculation using a Kane's band model which incorporates strain effects [9], and the radiative recombination model based on Fermi's golden rule with an assumption that there is no electric field that causes non-uniform charge distribution in the MQW active region. The material parameters such as Luttinger's parameters and energy gap have been estimated from those of the constituent binaries by linear interpolation. Effective mass of conduction electrons and heavy- and light-holes of the unstrained InAsSb, and energy gaps of InAsSb, InAs, InPAsSb are estimated to be 0.023 m_o, 0.25 m_o, 0.025 m_o, 0.32 eV, 0.41 eV, and 0.51 eV, respectively, where m_o is the free-electron effective mass. Using these material parameters, we obtained

J_{th} ~ 78 A/cm^2 and 50 A/cm^2 at 90 K for a cavity length of 1200 μm, for DH and MQW lasers, respectively, which are in a close agreement with experiment [10]. This indicates that the compressive strain effect predicted by the simple strain model is indeed manifested in the MQW lasers.

Figures 4 show that J_{th} of MQW lasers at 78 K is higher than that at 90 K. This fact was also consistently found in all lasers with various cavity lengths examined. This is in contrast to the results of DH lasers where J_{th} increases with temperature for the entire temperature range with J_{th} = 40~50 A/cm^2 at 78 K [6] (Figs. 4). The anomalous temperature dependence of J_{th} was found in all of the MQW laser diodes examined (about 10 diodes). The anomalous temperature dependence of J_{th} was also observed in similar InAsSb/InPAsSb MQW lasers fabricated by Kurtz *et al.* [1]. We suspect that the higher J_{th} at 78 K than at 90 K may come from insufficient thermalization of carriers in the wells at low temperature, prohibiting efficient carriers transport between the wells, and causing non-uniform carrier distribution. Because of the anomalous temperature dependence, T_o for the MQW lasers for the temperature range between 78 and 120 K is about 100 K on average, which is about 3 times higher than those of DH lasers (where T_o is defined by $(T_1 - T_2)^{-1} \log J_1 / J_2$ with T_1 =78 and T_2 =120 K).

In conclusion, we have shown direct evidence of the superior performance of MQW InAsSb lasers over that of DH lasers. A comparison with theory strongly indicates that the reduction of J_{th} comes from the reduced density of states resulting from the compressive strain on the active quantum well region. About 2 times lower J_{th} has been obtained in MQW lasers compared to bulk DH lasers for temperature range of 90 to 140 K. Maximum peak power of 1 W, differential efficiency over 65 % up to 155 K and maximum operating temperature of 220 K have been demonstrated from the uncoated MQW lasers. The lower J_{th} of MQW lasers compared to DH lasers can be quantitatively explained by the lower density of states and differential efficiency due to the compressive strain.

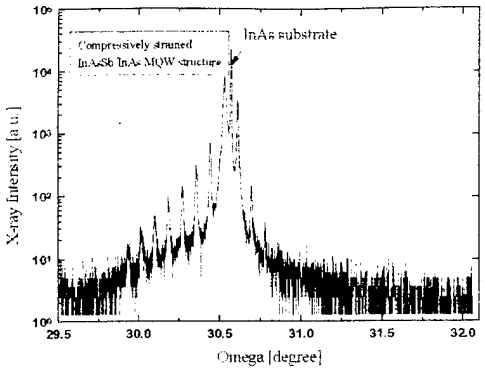

Fig. 1 A (004) x-ray rocking curve for the laser structure; (inset) the schematic diagram of the MQW structure

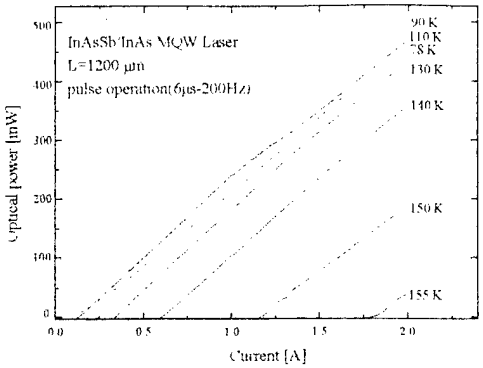

Fig.2 The optical power vs. injection current curves (*P-I* curves) of one of the MQW lasers measured at wide range of temperature (78 to 155 K)

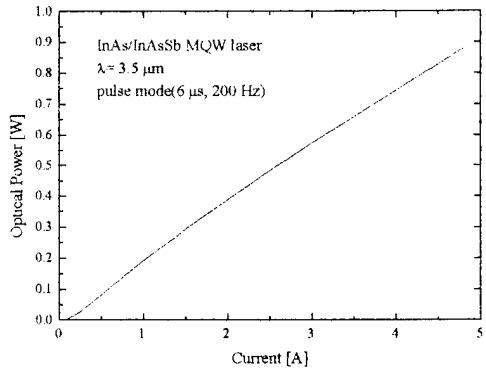

Fig.3 The optical power vs. injection current curve (*P-I* curve) of one of the MQW lasers measured at 78 K

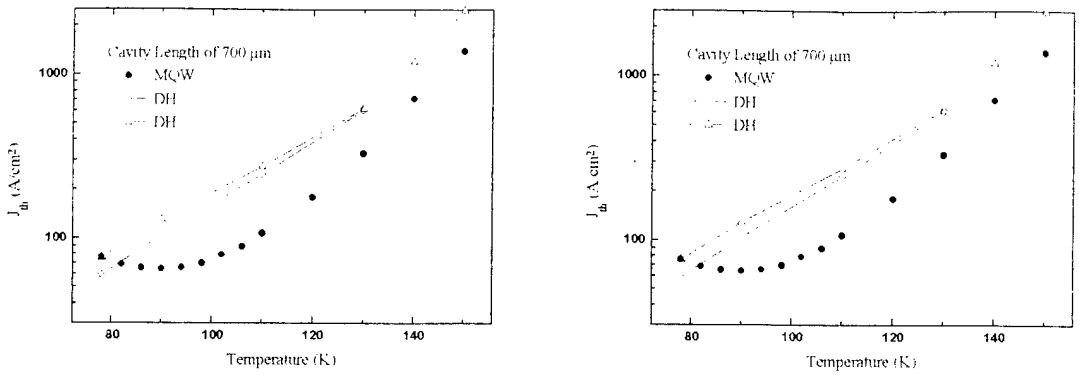

Fig 4. Temperature dependence of J_{th} of MQW lasers compared to that of DH lasers for cavity lengths of (a) 700 μm and (b) 1200 μm

References

[1] S. R. Kurtz, R. M. Biefield, A. A. Allerman, A. J. Howard, M. H. Crawford, and M. W. Pelczynski, Appl. Phys. Lett. **68**, 1332 (1996)

[2] H. K. Choi, and G. W. Turner, Appl. Phys. Lett. **67**, 332 (1995)

[3] A. Popov, V. Sherstnev, and Y. Yakovlev, R. Mucke, and P. Werle, Appl. Phys. Lett. **68**, 2790 (1996)

[4] M. Aydaraliev, N. V. Zotova, S. A. Karandashov, B. A. Matveev, N. M. Stus' and G. N. Talalakin, Semicond. Sci. Technol. **8**, 157 (1993)

[5] For example see S. Colak, R. Eppenga, and M. F. H. Schuurmans, IEEE J. Quantum Electron. **QE-23**, 960 (1987); P. A. Chen and C. Y. Chang, J. Appl. Phys. **76**, 85 (1994)

[6] J. Diaz, B. Lane, A. Rybaltowski, H. J. Yi, and M. Razeghi (to be published, IEEE Photon. Technol. Lett.)

[7] In the lasers based on inter-subband transition [8], η_d as high as 60 % up to room temperature has already been reported.

[8] J. Faist, F. Capasso, C. Sirtori, D. L. Sivco, J. N. Baillargeon, A. L. Hutchinson, S. G. Chu, and A. Y. Cho, Appl. Phys. Lett. **68**, 3680 (1996)

[9] D. Gershoni, C. Henry, and G. Baraff, IEEE J. Quantum Electron. **QE-29**, 2433 (1993)

[10] The agreement with experiment for short cavity lasers is less perfect, presumably because of the gain saturation effect due to inhomogeneity of the active region discussed previously [6].